A FIELD VALIDATED SURROGATE CROP MODEL FOR PREDICTING ROOTZONE MOISTURE AND SALT CONTENT IN REGIONS WITH SHALLOW GROUNDWATER

Zhongyi Liu[1], Zailin Huo[1]*, Chaozi Wang[1], Limin Zhang[2], Xianghao Wang[1], Guanhua Huang[1], Xu Xu[1], Tammo Siert Steenhuis[3]*

1. Center for Agricultural Water Research in China, China Agricultural University, Beijing, 100083, PR China

2. School of Water Resources and Environment, China University of Geosciences, Beijing, 100083, PR, China

3. Department of Biological and Environmental Engineering, Cornell University, Ithaca, NY, USA.

Correspondence to: Zailin Huo (huozl@cau.edu.cn)

Tammo S. Steenhuis (tss1@cornell.edu)

Abstract

Optimum management of irrigated crops in regions with shallow saline groundwater requires a careful balance between application of irrigation water and upward movement of salinity from the groundwater. Few field validated surrogate models are available to aid in the management of irrigation water under shallow groundwater conditions. The objective of this research is to develop a model that can aid in the management using a minimum of input data that is field validated. In this paper a 2-year field experiment was carried out in the Hetao irrigation district in Inner Mongolia, China and a physically based integrated surrogate model for arid irrigated areas with shallow groundwater was developed and validated with the collected field data. The integrated model that links crop growth with available water and salinity in the vadose zone is called Evaluation of the Performance of Irrigated Crops and Soils (EPICS). EPICS recognizes that field capacity is reached when the matric potential is equal to the height above the groundwater table and thus not by a limiting hydraulic conductivity. In the field experiment, soil moisture contents and soil salt conductivity at 5 depths in the top 100 cm, groundwater depth, crop height, and leaf area index were measured in 2017 and 2018. The field results were used for calibration and validation of EPICS. Simulated and observed data fitted generally well during both calibration and validation. The EPICS model that can predict crop growth, soil water, groundwater depth and soil salinity can aid in optimizing water management in irrigation districts with shallow aquifers.

Key words: Surrogate hydrological model, irrigated crops, shallow aquifer

Nomenclature

ET_0	Reference evapotranspiration (mm)
ET_P	Potential evapotranspiration (mm)
E_p	Potential evaporation (mm)
T_p	Potential transpiration (mm)
E_a	Actual evaporation (mm)
T_a	Actual transpiration (mm)
K_c	Crop coefficient ()
τ	Development stage of the leaf canopy ()
r_T	Root function for transpiration ()
r_E	Root function for transpiration ()
j	Number of soil layer ()
LAI	Leaf area index ()
T_{mean}	Mean daily temperature (℃)
T_{mx}	Maximum daily temperature (℃)
T_{mn}	Minimum daily temperature (℃)
LAI_{mx}	Maximum leaf area index
RD_{mx}	Maximum root depth (cm)
K_b	Dimensionless canopy extinction coefficient
PHU	Total potential heat units required for crop maturation (℃)
Z_{1j}	Depth of the upper boundaries of soil layer j (cm)
Z_{2j}	Depth of the lower boundaries of the soil layer for $r_E(j,t)$; root depth or the lower boundaries of the soil layer for $r_T(j,t)$ (cm)
δ	Water use distribution parameter
k_E	Water stress coefficient for evaporation
k_T	Water stress coefficient for transpiration
θ	Soil moisture content ($cm^{-3}\,cm^{-3}$)
θ_{fc}	Soil moisture content at field capacity ($cm^{-3}\,cm^{-3}$)
θ_r	Soil moisture content at wilting point ($cm^{-3}\,cm^{-3}$)
f_{shape}	Shape factor of k_T curve ()
p	Fraction of readily available soil water relative to the total available soil water
S	Salt stress coefficient ()
B	Crop specific parameter (%)
k_y	Factor that affects crop yield
EC_e	Electrical conductivity of the soil saturation extract ($mS\,cm^{-1}$)
$EC_{ethreshold}$	Threshold of the electrical conductivity of the soil saturation extract when the crop yield becomes affected by salt ($mS\,cm^{-1}$)
$EC_{1:5}$	Electrical conductivity of the soil extract that soil samples mixed with distilled water in a proportion of 1:5 ($mS\,cm^{-1}$)
θ_s	Soil moisture content at saturation ($cm^{-3}\,cm^{-3}$)
φ_b	Bubbling pressure (cm)
φ_m	Matric potential (cm)
λ	Pore size distribution index
h	Groundwater depth (cm)
z	Depth of the point below the soil surface (cm)
$W_{fc}(h)$	Total water content at field capacity of the soil profile over a prescribed depth (cm)
L(j)	Height of layer j (cm)
μ	Drainable porosity
P	Precipitation (mm)
I	Irrigation (mm)
n	Number of soil layers
R_{gw}	Percolation to groundwater (mm)
$R_w(j-1,t)$	Percolation rate to layer j from layer j-1 at day t (mm)
C(j,t)	Salt concentration of layer j at day t ($g\,L^{-1}$)
C_I	Salt concentration of irrigation water ($g\,L^{-1}$)
C_{gw}	Salt concentration of groundwater ($g\,L^{-1}$)
U_{gw}	Actual upward flux of groundwater (mm)
$U_{gw,max}$	Maximum upward flux of groundwater (mm)
a	Constant used for calculation of $U_{gw,max}$ ()
b	Constant used for calculation of $U_{gw,max}$()

44

1. Introduction

Irrigation water is a scarce resource, especially in arid and semi-arid areas of the world. Irrigation improves quality and quantity of food production; however, excess irrigation and salinization remain one of the key challenges. Almost 20% of the irrigated land in the world is affected by salinization and this percentage is still on the rise (Li et al., 2014). Soil salinization and water shortages, especially associated with surface irrigated agriculture in arid to semi-arid areas, is a threat to the well-being of local communities in these areas (Dehaan and Taylor, 2002; Rengasamy, 2006).

In arid and semi-arid areas where people divert surface water for flood irrigation and have poor drainage infrastructures, the groundwater table is close to the surface because more water has been applied than crop evapotranspiration. Capillary rise of the shallow groundwater can be used to supplement irrigation and thereby, in closed basins, can possibly save water for irrigating additional areas downstream (Gao et al., 2015; Yeh and Famiglietti, 2009; Luo and Sophocleous, 2010.). However, at the same time, capillary upward moving water carries salt from the groundwater increasing the salt in the upper layers of the soil leading to soil degradation and possibly decreasing yields and change of crop patterns to more salt tolerant crops (Guo et al., 2018; Huang et al., 2018). The leaching of salt with irrigation water is necessary and useful for irrigated agriculture (Letey et al., 2011). In north China, the fields are commonly irrigated in the autumn before soil freezing to leach salts and provide water for first growth after seeding in the following year (Feng et al., 2005).

Tradeoffs between irrigation practices and soil salinity were studied by a lot of

researchers (Hanson et al., 2008; Pereira et al., 2002, 2009; Minhas et al., 2020). Minhas et al. (2020) give a brief review of crop evapotranspiration and water management issues when coping with salinity in irrigated agriculture. Phogat et al. (2020) assessed the effects of long-term irrigation on salt build-up in the soil under unheated greenhouse conditions by the UNSA-TCHEM and HYDRUS-1D (Phogat et al., 2020).

Therefore, understanding the interaction of improved crop yield, soil salinization and decreased surface irrigation is important to the sustainability of the surface irrigation water systems in arid and semi-arid areas. This will require experimentation under realistic farmers' field conditions, as well as modeling to extend the findings beyond the plot scale.

Field scale models for water, solute transport and crop growth are widely available. Crop growth models use either empirical functions or model the underlying physiological processes (Liu, 2009). Models widely used for simulating crop growth are EPIC (Williams et al., 1989), DSSAT (Uehara, 1989), WOFOST (Diepen et al., 1989) and AquaCrop (Hsiao et al., 2009; Raes et al., 2009; Steduto et al., 2009). Models that focus on water and solute movement in the vadose zone using some form of Richards' equation are HYDRUS (Šimůnek et al., 1998) and SWAP (Dam et al., 1997). Models that integrate crop growth and water-solute movement processes are SWAP-WOFOST (Hu et al., 2019), SWAP-EPIC (Xu et al., 2015; Xu et al., 2016), HYDRUS-EPIC ((Wang et al., 2015), and HYDRUS-DSSAT (Shelia et al., 2018). These integrated models require input data that are usually not available when

applied over extended areas (Liu et al., 2009; Xu et al., 2016; Hu et al., 2019). The EPIC crop growth model is often preferred in integrated crop growth hydrology models because it requires relatively few input data and is accurate (Wang et al., 2014; Xu et al., 2013; Chen et al., 2019).

There is a tendency with the advancement of computer technology to include more physical processes in these models (Asher et al., 2015; Doherty and Simmons, 2013; Leube et al., 2012). Detailed spatial input of soil hydrological properties and crop growth are required to take advantage of the model complexity (Flint et al., 2002; Rosa et al., 2012). This greater model complexity, both in space and time, requires longer model run times, especially for the time-dependent models (Leube et al., 2012). These models are useful for research purposes but for actual field applications, the required input data are not available and expensive to obtain. In such cases, simpler surrogate models are a good alternative (Blanning, 1975; Willcox and Peraire, 2002; Regis and Shoemaker, 2005). Surrogate models run faster and are as accurate as the complex models for a specific problem (shallow groundwater here) but not as versatile as the more complex models that can be applied over a wide range of conditions (Asher et al., 2015).

Simple surrogate models are abundant in China for areas where the groundwater is deeper than approximately 10 m (Kendy et al., 2003; Chen et al., 2010; Ma et al., 2013; Li et al., 2017; Wu et al., 2016), but are limited and relatively scarce for areas where the groundwater is near the surface in the arid to semi-arid areas (Xue et al., 2018; Gao et al., 2017; Liu et al., 2019). In these areas with shallow aquifer, the

upward groundwater flux from groundwater is an important factor in meeting the evapotranspiration demand of the crop (Babajimopoulos et al., 2007; Yeh and Famiglietti, 2009). The advantage of applying surrogate models in areas with shallow aquifer is that they can simulate the hydrological process with fewer parameters using with simpler and computationally less demanding mathematical relationships than the traditional finite element or difference models (Wu et al., 2016; Razavi et al., 2012).

The change in matric potential is often ignored in these surrogate models for soils with a deep groundwater table. However, for areas with shallow aquifers (i.e., less than approximately 3 m), the matric potential cannot be ignored. The flow of water is upward when the absolute value of matric potential is greater than the groundwater depth or downward when it is less than the groundwater depth (Gardner, 1958; Gardner et al., 1970a; b; Steenhuis et al., 1988). The field capacity in these soils is reached when the hydraulic gradient is constant (i.e., the constant value of sum of matric potential and gravity potential). In this case, the soil water is in equilibrium and no flow occurs.

Xue et al. (2018) and Gao et al. (2017), developed models for the shallow groundwater, but used field capacities and drainable porosities that were calibrated and independent of the depth of the groundwater. This is inexact when the groundwater is close to the surface. Liu et al. (2019), used for simulating shallow groundwater the same type of model as described in this paper but calibrated crop evaporation and did not simulate the salt concentrations in the soil. This made their model less useful for practical application.

Because of the shortcomings in the above complex models, we avoided the use of a constant drainable porosity and considered the crop growth and thus improved the surrogate model in our last study (Liu et al., 2019). The objective of this research was to develop a field validated surrogate model that could be used to simulate the water and salt movement and crop growth in irrigated areas with shallow groundwater and salinized soil with a minimum of input parameters. To validate the surrogate model, we performed a 2-year field experiment in the Hetao irrigation district that investigated the change in soil salinity, moisture content, groundwater depth and maize and sunflower growth during the growing season.

In the following section we present first the theoretical background of the surrogate model. The model consists of crop growth module and a vadose zone module. This is followed by detailed description of the two-year field experiments started in 2017 in the Hetao irrigation district where maize and sunflower were irrigated by flooding the field. The experimental results consisting of climate data, irrigation application, crop growth parameters, moisture and salt content and groundwater depth are used to calibrate and validate the model.

2. Model description

2.1 Introduction of the model

In a recent study, we presented a surrogate model for the vadose zone with shallow groundwater using the novel concept that the moisture content at field capacity is a unique function of the groundwater depth after irrigation or precipitation that wets up the entire soil profile. The model, called the Shallow Vadose Groundwater model, is

applied directly to surface irrigated districts where the groundwater is within 3.3 m from the soil surface (Liu et al. 2019). The model was a proof of concept with calibrated values for evapotranspiration and soil salinity which was not simulated.

To make the Shallow Vadose Groundwater model more physically realistic, we added a crop growth model and included the effect of salinity and moisture content on evaporation and transpiration directly in this study. The new model that combines parts of the EPIC (Erosion Productivity Impact Calculator, Williams et al., 1989) with Shallow Vadose Groundwater model is called the *Evaluation of the Performance of Irrigated Crops and Soils* (EPICS).

2.2 Structure of the EPICS model

In the EPICS model, the soil profile is divided into five layers of 20 cm (from the soil surface down) and a sixth layer that stretches from the 100 cm depth to the water table below (Fig. 1).

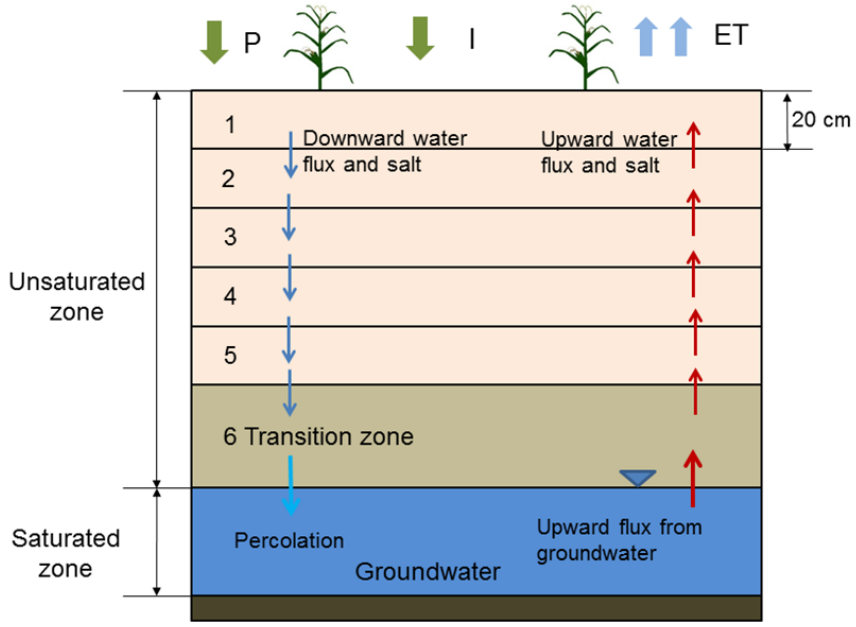

Figure 1. Schematic diagram of model components and water movement

The moisture content and salt content are calculated for each day (Fig.1). All flow takes place within the day and the water and salt content are in “equilibrium” (i.e., fluxes are zero) at the end of the day for which the calculations are made. Daily fluxes considered in the vadose model are the following: at the surface, the fluxes are irrigation, both irrigation water, $I(t)$, and salt, $S_0(t)$, and precipitation, $P(t)$, and for each layer, j, on days with irrigation and rainfall, the downward flux of water, $R_w(j,t)$, and salt, $S(j,t)$, between the layers. On days without water input at the soil surface, an upward groundwater flux $U(j,h,t)$, and salt, $S(j,t)$ are considered. The flux to the surface depends on the groundwater depth. Finally, transpiration, $T(j,t)$, removes water from the layers with roots of the crops and evaporation, $E(j,t)$, from all layers.

The EPICS model consists of two modules: the VADOSE module and the CROP module. The two modules are linked through the evapotranspiration flux in the soil (Fig. 2).

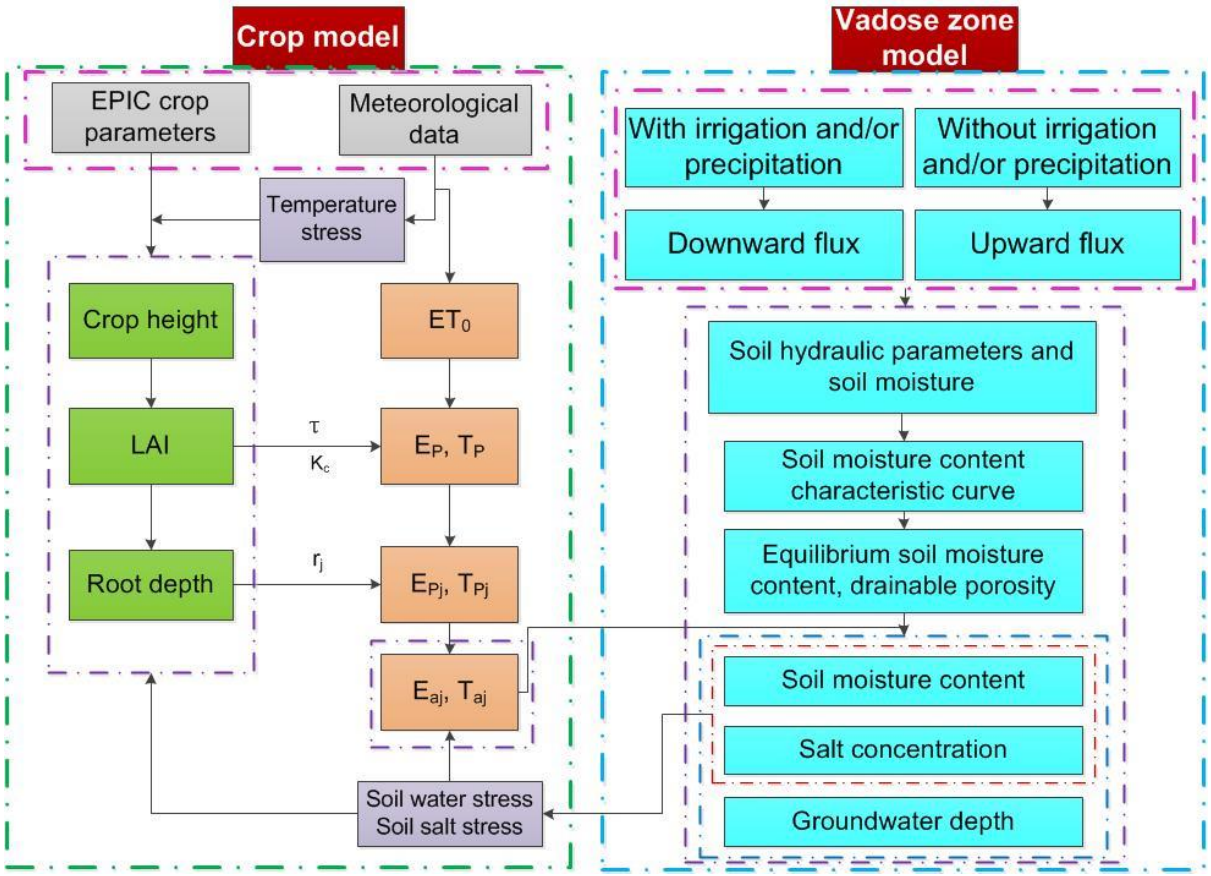

Figure 2. Schematic diagram of the linked novel Shallow Aquifer-Vadose zone surrogate module and EPIC module. Note: ET_0 is the reference evapotranspiration, E_p and T_p are the potential evaporation and potential transpiration, E_a and T_a are the actual evaporation and actual transpiration, K_c is the crop coefficient, τ is the development stage of the leaf canopy, and r_j is the root function of soil layer j.

The CROP module employs functions of the EPIC model (Williams et al., 1989) and root growth distribution (Novak, 1987; Kendy et al., 2003; Chen et al. 2019). The CROP module calculates daily values of crop height, root depth and leaf area index (LAI) based on climatic data (Fig. 2).

The VADOSE module calculates the moisture and salt content in the root zone and the upward movement of the groundwater (Fig.2). Field capacity varies with depth and is a function of the (shallow) groundwater depth and the soil characteristic curve (Liu et al., 2019). Moisture contents become less than field capacity when the

198 upward flux is less than the actual evapotranspiration.

199 Finally, the link between the VADOSE and the CROP modules is achieved by
200 calculating the actual evapotranspiration with parameters of both modules consisting
201 of the moisture content and the salt content simulated in the VADOSE module and
202 root distribution and potential evapotranspiration in the CROP module (Fig. 2).

203 2.3 Theoretical background of the EPICS model

204 In the next section, the equations of the CROP in the VADOSE modules are
205 presented. The calculations are carried out sequentially on a daily time step. This
206 model predicts field daily soil water, salt content and crop growth, which are critical
207 parameters for irrigation water management. For field and regional water
208 management and irrigation policy development, resolution of daily time step is
209 sufficient. Finer resolution is not needed for managing water and salt content for
210 irrigation. In the first step, the actual evaporation and transpiration are calculated for
211 each layer in the model. Next, the moisture content and salt content are adjusted for
212 the various fluxes. Since the equations for the downward movement on days of
213 rainfall and/or irrigation are different than for upward movement from the groundwater
214 on the remaining days, we present the upward and downward movement in separate
215 sections. The code was written in Matlab 2014Ra and Microsoft Excel was used for
216 data input and output.

217 2.3.1 CROP module

218 The crop module uses functions of EPIC (Erosion Productivity Impact Calculator,
219 Williams et al., 1989) to calculate leaf area index, LAI, crop height and the root depth

220 (green boxes in Fig. 2), and the potential transpiration, *T,* and evaporation, *E* (orange
221 boxes in Fig, 2). Input data for the CROP module included: mean daily temperature
222 (T_{mean}), maximum daily temperature (T_{mx}), minimum daily temperature (T_{mn}),
223 maximum crop height (H_{mx}), maximum LAI (LAI_{mx}), maximum root depth (RD_{mx}),
224 dimensionless canopy extinction coefficient (K_b), and total potential heat units
225 required for crop maturation (*PHU*).

226 The potential rates of evaporation, $E_P(j,t)$, and transpiration,$T_P(j,t)$, of different
227 layers are derived from the total rates and a root function that determines the
228 distribution of roots in the vadose zone

229 $$T_P(j,t) = r_T(j,t)T_p(t) \quad (1a)$$

230 $$E_p(j,t) = r_E(j,t)E_p(t) \quad (1b)$$

231 where j is the number of soil layers and t is the day number, $T_P(t)$ is the total
232 potential transpiration and $E_P(t)$ is the total potential transpiration at time, *t*. Both are
233 calculated with the CROP module (S1 in the supplementary material). Root functions
234 (Sau et al., 2004; Delonge et al., 2012) were used to calculate transpiration and
235 evaporation of different soil layer. $r_T(j,t)$ is the root function for the transpiration and
236 $r_E(j,t)$ is the root function for the evaporation. Both have the same general equation
237 but with a different value for the constant δ.

238 $$r_T(j,t) = \left[\frac{1}{1-exp(-\delta)}\right]\left\{exp\left[-\delta\left(\frac{Z_{1j}}{Z_{2j}}\right)\right]\left[1-exp\left(-\delta\frac{Z_{2j}-Z_{1j}}{Z_r}\right)\right]\right\} \quad (2a)$$

239 $$r_E(j,t) = \left[\frac{1}{1-exp(-\delta)}\right]\left\{exp\left[-\delta\left(\frac{Z_{1j}}{Z_{2j}}\right)\right]\left[1-exp\left(-\delta\frac{Z_{2j}-Z_{1j}}{Z_r}\right)\right]\right\} \quad (2b)$$

240 Where z_{1j} is the depth of the upper boundaries of the soil layer *j*. For $r_T(j,t)$ if the

root depth is smaller than the lower boundaries of the soil layer *j*, Z_{2j} is equal to the root depth and if the root depth is greater than the lower boundaries of the soil layer *j*, Z_{2j} is the depth of the lower boundaries of the soil layer *j*. For $r_E(j,t)$, Z_{2j} is depth of the lower boundaries of the soil layer *j*. Z_r is the root zone depth and δ is the water use distribution parameter. Note that the sum of $r_T(j,t)$ of all soil layers is equal to 1. In the study of Novark (1987), the value of δ for corn is 3.64 and we used this value. To obtain $r_E(j,t)$, δ was set to 10 (Chen et al., 2019; Kendy et al., 2003). Sunflower root function simulation employed the same δ values as for maize.

The actual evaporation rates, $E_a(j,t)$, and transpiration, $T_a(j,t)$, for each soil layer, *j,* at time, *t,* are calculated as a proportion of the potential values as:

$$E_a(j,t) = k_E(j,t)E_p(j,t) \quad (3a)$$

$$T_a(j,t) = k_T(j,t)S(j,t)T_p(j,t) \quad (3b)$$

where $k_E(j)$ and $k_T(j)$ are water stress coefficients and $S(j)$ is a salt stress coefficient. According to Raes et al. (2009), the water stress coefficients are

$$k_E(j,t) = \exp\left(-2.5\frac{\theta_{fc}(j)-\theta(j,t)}{\theta_{fc}(j)-\theta_r(j)}\right) \qquad \theta \le \theta_{fc} \quad (4a)$$

$$k_E(j,t) = 1 \qquad \theta > \theta_{fc} \quad (4b)$$

where $\theta_{fc}(j)$ is the moisture content at field capacity for layer *j*, or when the conductivity becomes limiting and $\theta_r(j)$ is the moisture content at wilting point, $\theta(j,t)$ is the soil moisture content for layer *j* at time *t*.

Then water stress coefficient in Eq. 3b is:

$$k_T(j,t) = 1 - \frac{\exp\left[\left(1-\frac{\theta(j,t)-\theta_r(j)}{(1-p)\left[\theta_{fc}(j)-\theta_r(j)\right]}\right)f_{shape}\right]-1}{\exp\left(f_{shape}\right)-1} \quad \theta \le \theta_{fc} \quad (5a)$$

$$k_T(j,t) = 1 \qquad \theta > \theta_{fc} \quad (5b)$$

where f_{shape} is the shape factor of $k_T(j,t)$ curve, p is the fraction of readily available soil water relative to the total available soil water. Finally, the salt stress coefficient $S(j,t)$ for each layer in Eq 3b can be calculated as (Allen et al., 1998; Xue et al., 2018):

$$S(j,t) = 1 - \frac{B}{100\ k_y}(EC_e(j,t) - EC_{ethreshold}) \quad (6)$$

where k_y is the factor that affects the yield, EC_e is the electrical conductivity of the soil saturation extract (mS cm^{-1}), $EC_{ethreshold}$ is the calibrated threshold of the electrical conductivity of the soil saturation extract when the crop yield becomes affected by salt (mS cm^{-1}), and *B* is the calibrated crop specific parameter that describes the decrease rate of crop yield when EC_e increases per unit below the threshold. The electrical conductivity of the soil saturation extract can be calculated as (Rhoades et al., 1989):

$$EC_e = 1.33 + 5.88 \times EC_{1:5} \quad (7)$$

where $EC_{1:5}$ is the electrical conductivity of the soil extract that soil samples mixed with distilled water in a proportion of 1:5.

2.3.2 VADOSE Module

For modeling the daily soil moisture content and groundwater depth, first we need to calculate the soil moisture content at field capacity and the drainable porosity based on the soil moisture characteristic curve. Besides, we assume that the water and salt moves downward on rainy and/or irrigation days, while the water and salt moves upward on days without rain and/or irrigation.

284 2.3.2.1 Parameters based on soil moisture characteristic curve for modeling

285 Moisture content at field capacity

286 Field capacity with a shallow groundwater is different than in soils with deep
287 groundwater where water stops moving when the hydraulic conductivity becomes
288 limiting at -33 kPa. When the groundwater is shallow, the hydraulic conductivity is not
289 limiting and the water stops moving when the hydraulic potential is constant and thus
290 the matric potential is equal to the height above the water table (Gardner 1958;
291 Gardner et al.,1970a, b; Steenhuis et al., 1988; Liu et al., 2019). Assuming a unique
292 relationship between moisture content at field capacity and matric potential (i.e. soil
293 characteristic curve), the moisture content at field capacity at any point above the
294 water table is a unique function of the water table depth. Thus, any water added
295 above field capacity will drain downward. When the groundwater is recharged, the
296 water table will rise and increase the moisture contents at field capacity throughout
297 the profile.

298 The moisture contents at field capacity were found by Liu et al. (2019) using the
299 simplified Brooks and Corey soil characteristic curve (Brooks and Corey, 1964)

300 $$\theta = \theta_s \left[\frac{\varphi_m}{\varphi_b}\right]^{-\lambda} \qquad for\ |\varphi_m| > |\varphi_b| \qquad (8a)$$

301 $$\theta = \theta_s \qquad for\ |\varphi_m| \leq |\varphi_b| \qquad (8b)$$

302 in which θ is the soil moisture content ($cm^3\ cm^{-3}$), θ_s is the saturated moisture
303 content ($cm^3\ cm^{-3}$), φ_b is the bubbling pressure (cm), φ_m is the matric potential (cm),
304 and λ is the pore size distribution index. The moisture content at field capacity,
305 $\theta_{fc}(z, h)$, for any point, z, from the surface water for a groundwater at depth, h, can be

306 expressed as (Liu et al. 2019)

307 $$\theta_{fc}(z,h) = \theta_s(z)\left[\frac{h-z}{\varphi_b}\right]^{-\lambda} \qquad for\ |h-z| > |\varphi_b(z)| \quad (9a)$$

308 $$\theta_{fc}(z,h) = \theta_s(z) \qquad for\ |h-z| \leq |\varphi_b(z)| \quad (9b)$$

309 where *h* (cm) is the depth of the groundwater and *z* (cm) is the depth of the point
310 below the soil surface. Thus (*h-z)* is the height above the groundwater and this is
311 equal to the matric potential for soil moisture content at field capacity.

312 For shallow groundwater, the matric potential at the surface is -33kPa when the
313 groundwater is 3.3 m depth. For this matric potential, as mentioned above, the
314 conductivity becomes limiting. This depth of the groundwater is therefore the lower
315 limit over which the VADOSE module is valid.

316 Evapotranspiration can lower the soil moisture content below field capacity. Thus,
317 the maximum moisture content in the VADOSE module is determined by the soil
318 characteristic curve and the height of the groundwater table, and the minimum is the
319 wilting point that can be obtained by evapotranspiration by the crop. Note that the
320 saturated hydraulic conductivity does not play a role in determining the moisture
321 content because inherently it is assumed that it is not limiting in the distribution of the
322 water.

323 Drainable porosity

324 The drainable porosity is a crucial parameter in modelling the groundwater depth and
325 soil moisture content. According to the soil water characteristic curve at field capacity,
326 the drainable porosity can be expressed as a function of the depth. The drainable

porosity is obtained by calculating the field capacity, $W_{fc}(h)$ (cm) for each layer at all groundwater depths. The total water content at field capacity of the soil profile over a prescribed depth with a water table at depth *h* can be expressed as:

$$W_{fc}(h) = \sum_{j=1}^{n} \left[L(j)\, \theta_{fc}(j,h) \right] \qquad (10)$$

where $\theta_{fc}(j,h)$ is the average moisture content at field capacity of layer j that can be found by integrating Eq. 8 from the upper to the lower boundary of the layer and dividing by the length *L(j)* which is the height of layer *j*. The matric potential at the boundary is equal to the height above the water table. The drainable porosity, $\mu(h)$, which is a function of the groundwater depth *h,* can simply be found as the difference in water content when the water table is lowered over a distance of $2\Delta h$.

$$\mu(h) = \frac{W_{fc}(h+\Delta h) - W_{fc}(h-\Delta h)}{2\Delta h} \qquad (11)$$

where $\Delta h = 0.5L(j)$ (cm).

2.3.2.2 Downward flux (at times of irrigation and/or precipitation) and model output

During the downward flux period, the upward water flux from groundwater is zero. Under this condition, the model can output the daily soil moisture content of different soil layers, the percolation from each soil layer to the soil layer beneath, the discharge from soil water to groundwater, the salt concentration of groundwater and of soil water in each soil layer, and the groundwater depth.

Water

A downward flux occurs when either the precipitation or irrigation is greater than the actual evapotranspiration. In this case, upward flux will not occur because the actual

evapotranspiration is subtracted from the input at the surface. We consider two cases when the groundwater is being recharged and when it is not.

When the net flux at the surface (irrigation plus rainfall minus actual evapotranspiration) is greater than that needed to bring the soil up to equilibrium moisture content, the groundwater will be recharged and the distance of the groundwater to soil surface decreases and the moisture content will be equal to the moisture at field capacity. The fluxes from one layer to the next can be calculated simply by summing the amount of water needed to fill up each layer below to the new moisture content at field capacity. Hence, the percolation to groundwater, $R_{gw}(t)$, can be expressed as:

$$R_{gw}(t) = P(t) + I(t) - E_a(t) - T_a(t) - \sum_{j=1}^{n} \frac{\left[\theta_{fc}(j,h) - \theta(j,t-\Delta t)\right]L(j)}{\Delta t} \qquad (12)$$

where *n* is the total number of layers, $\theta(j,t)$ is the average soil moisture content in day *t* of layer *j* ($cm^3\ cm^{-3}$), $E_a(t)$ is the actual evaporation (mm), $T_a(t)$ is the actual transpiration (mm), $P(t)$ is the precipitation (mm), and $I(t)$ is the irrigation (mm).

When the groundwater is not recharged, the rainfall and the irrigation are added to uppermost soil layer and when the soil moisture content will be brought up to the field capacity and the excess water will infiltrate to next soil layer bringing it up to field capacity. This process continues until all the rainwater is distributed. Formally the soil moisture can be expressed as

$$\theta(j,t) = min\left[\theta_{fc}(j,h), \left[\theta(j,t-\Delta t) + \frac{R_w(j-1,t)\,\Delta t}{L(j)}\right]\right] \qquad (13)$$

where $\theta(j,t)$ is the average soil moisture content in day t of layer j ($cm^3\ cm^{-3}$),

$R_w(j-1,t)$ is the percolation rate to layer *j* (mm) and can be found with Eq 12 by replacing *j-1* for n in the summation sign.

$$R_w(j-1,t) = P(t) + I(t) - E_a(t) - T_a(t) - \sum_{1}^{j-1} \frac{\left[\theta_{fc}(j,h) - \theta(j,t-\Delta t)\right]L(j)}{\Delta t} \quad (14)$$

For the uppermost soil layer, the water percolation can be expressed as

$$R_w(0,t) = I(t) + P(t) - E_a(t) - T_a(t) \quad (15)$$

Salinity

The salt concentration for layer j can be expressed by a simple mass balance as:

$$C(j,t) = \frac{\theta(j,t-\Delta t)\, C(j,t-\Delta t)L(j) + [R_w(j-1,t)\, C(j-1,t) - R_w(j,t)\, C(j,t)]\, \Delta t}{\theta(j,t)L(j)} \quad (16)$$

where $C(j,t)$ is the salt concentration of layer j at time t (g L^{-1}). The equation can be rewritten as an explicit function of $C(j,t)$

$$C(j,t) = \left[\frac{\theta(j,t)L(j)}{1 + R_w(j,t)\ \Delta t}\right]\left[\frac{\theta(j,t-\Delta t)\, C(j,t-\Delta t)L(j) + R_w(j-1,t)\, C(j-1,t)\, \Delta t}{\theta(j,t)L(j)}\right] \quad (17)$$

For the surface layer j=1, we obtain

$$C(1,t) = \left[\frac{\theta(1,t)L(1)}{1 + R_w(1,t)\Delta t}\right]\left[\frac{\theta(1,t)L(1)}{1 + R_w(1,t)\Delta t}\frac{\theta(j,t-\Delta t)\, C(j,t-\Delta t)L(j) + I(t)\, C_I\, \Delta t}{\theta(j,t)L(j)}\right] \quad (18)$$

where C_I is the salt concentration in the irrigation water (g L^{-1}).

The salt concentration of the groundwater $C_{gw}(t)$ can be estimated as：

$$C_{gw}(t) = \frac{\left[G(t-1) \times C_{gw}(t-1) + C(5,t) \times R_w(t)\right]}{G(t-1) + R_w(t)} \quad (19)$$

Where $C(5,t)$ is the soil salinity concentration of the soil layer *5* on day *t* (g L^{-1}), $G(t-1)$ is the difference of the groundwater depth and the depth that the largest groundwater table fluctuations depth of groundwater table on day (*t-1)* (m) (Xue et al., 2018), $C_{gw}(t)$ is the soluble salt concentration of groundwater at day *t* (g L^{-1}).

2.3.2.3 Upward flux and model output

For the upward flux period, the downward water flux to groundwater is zero. The evapotranspiration leads to the decrease of soil moisture content in the vadose zone and lowers the groundwater table due to the upward movement of groundwater to crop root zone and soil surface. The soil moisture content is calculated by taking the difference of equilibrium moisture content associated with the change of groundwater depth. Under this condition, the model can output the daily soil moisture content of different soil layers, the upward groundwater flux, the groundwater depth, and the salt concentration of groundwater and of soil water in each soil layer.

Water

The groundwater upward flux, $U_{gw}(h,t)$, is limited by either the maximum upward flux of groundwater, $U_{gw,max}(h)$, or the actual evapotranspiration, formally stated as:

$$U_{gw}(h,t) = min\left[[E_a(t) + T_a(t)], U_{gw,max}(h)\right] \quad (20)$$

$$E_a(t) = \sum_{j=1}^{n} E_a(j,t) \quad (21)$$

$$T_a(t) = \sum_{j=1}^{n} T_a(j,t) \quad (22)$$

where $U_{gw,max}(h)$ is the actual upward flux from groundwater (mm), $E_a(t)$ is the actual evaporation at day *t* (mm), $T_a(t)$ is the actual transpiration at day *t* (mm), $E_a(j,t)$ is the actual evaporation at day *t* of layer *j* (mm) and $T_a(j,t)$ is the actual transpiration at day *t* of layer *j* (mm).

The maximum upward flux can be expressed as (Liu et al., 2019; Gardner et al., 1958)

$$U_{gw,max}(h) = \frac{a}{e^{bh} - 1} \quad (23)$$

where *a* and *b* are constants that need to be calibrated, *h* is the groundwater depth (cm).

Two cases are considered for determining the moisture contents of the layers depending on whether the actual evapotranspiration is greater or less than the maximum upward flux.

Case I: $U_{gw,max}(h) > E_a(t) + T_a(t)$

In this case, where the maximum upward flux is greater than the evaporative demand, the groundwater depth is updated

$$h(t) = h(t - \Delta t) + \frac{E_a(t) + T_a(t)}{\mu(\bar{h})} \quad (24)$$

where $\mu(\bar{h})$ is the average drainable porosity over the change in groundwater depth *h*. The moisture content after the change in groundwater depth becomes

$$\theta(j,t) = \theta(j,t - \Delta t) + \theta_{fc}\big(j,h(t)\big) - \theta_{fc}(j,h(t - \Delta t)) \quad (25)$$

Note that when the layer is at field capacity and the upward flux is equal to the evaporative flux, the layer remains at field capacity for the updated groundwater depth at time t.

Case II: $U_{gw,max}(h) \leq E_a(t) + T_a(t)$

In this case, the groundwater depth is updated

$$h(t) = h(t - \Delta t) + \frac{U_{gw,max}(h)}{\mu(\bar{h})} \quad (26)$$

When the upward flux is less than the sum of the actual evaporation and transpiration, the moisture content is updated with the difference between the two fluxes, $U_{gw,max}(h)$ and $[E_a(t) + T_a(t)]$, according to a predetermined distribution extraction of

water out of the root zone

$$\theta(j,t) = \theta(j,t-\Delta t)+\theta_{fc}\big(j,h(t)\big) - \theta_{fc}(j,h(t-\Delta t) - \frac{r(j)\big[E_a(t)+T_a(t)-U_{gw,max}(h)\big]}{L(j)} \quad (27)$$

The upward flux of water can be found by summing the differences in moisture content above the layer *j* similar to Eq 14, but starting the summation at the groundwater.

Salinity

The salt from groundwater is added to the soil layers according to the root function.

The soil salinity concentration in layer *j* at day *t* can be expressed as

$$\mathrm{C}(j,t) = \frac{\theta(j,t-\Delta t)\,C(j,t-\Delta t)L(j) + r(j,t)U_g(h,t)C_{gw}(t)}{\theta(j,t-\Delta t)L(j)+(\theta_{fc}\big(j,h(t)\big) - \theta_{fc}(j,h(t-\Delta t))L(j) - r(j,t)(E_a(t)+T_a(t)-U_{gw,max}(h))} \quad (28)$$

Since water is extracted from the reservoir that has the same concentration as in the reservoir, the concentration will not change, hence the equation used to estimate the groundwater salt concentration can be expressed as

$$C_{gw}(t) = C_{gw}(t-\Delta t) \quad (29)$$

3. Data collection

3.1 Study area

Field experiments were conducted in 2017 and 2018 in Shahaoqu experimental station in Jiefangzha sub-district, Heato irrigation district in Inner Mongolia, China (Fig. 3). Irrigation water originates from the Yellow River. The change of the irrigation water salinity is small and can be ignored during the crop growth period. The area has an arid continental climate. Mean annual precipitation is 155 mm a^{-1} of which 70% falls from June to September. Pan evaporation is 2000 mm a^{-1} (Xu et al., 2010). The mean

annual temperature is 7℃. The soils begin to freeze in the middle of November and to thaw in end of April or beginning of May. Maize, wheat and sunflower are the main crops in Jiefangzha sub-district and are grown with flood irrigation. The groundwater depth is between 0.5-3 m. Regional exchange of groundwater is minimal due to low gradient of 0.01-0.025 (Xu et al., 2010). Thus, the groundwater flows mainly vertically with minimum lateral flow in the regional scale. Over 50% of the total irrigated cropland, 5250 km^2 in the Hetao irrigation district in the Yellow River basin, is affected by salinity (Feng et al., 2005).

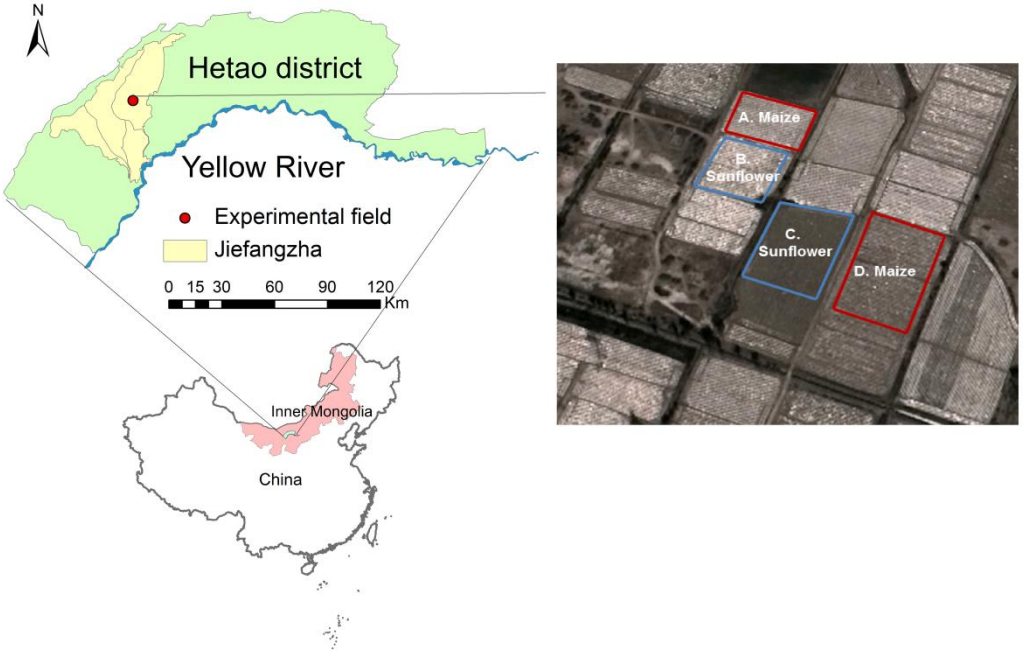

Figure 3. Location of the Shahaoqu experimental field (Note: The figure was downloaded from Google earth. The imagery is taken on April 8, 2019)

3.2 Field observations and data

The layout of the experimental fields is shown in Figure 3. The areas of fields A, B, C and D are 920, 2213, 1167, 1906 m^2, respectively. Field A and D were planted with maize on May 10 and harvested on September 30, 2017. In 2018, fields A and D were planted with gourds and were therefore not monitored in 2018. Fields B and C were

seeded with sunflower in both 2017 and 2018. The sunflower was planted on June 1, 2017 and June 5, 2018. Harvest was on September 15 in both years. The fields were irrigated by flooding the field ranging from two to five times during the growing season (Table 1). The salinity of the irrigation source water was measured three times during crop growth period and the mean value was used in the mass balance. The salinity of the irrigation source water is assumed unchanged. A well was installed in each experimental field to monitor the groundwater depth.

Table 1 Irrigation scheduling for the Shahaoqu experimental fields in 2017 and 2018

Field	Year	Irrigation events	Date	Irrigation depth (mm)
A (maize)	2017	1	5/30	100
		2	6/25	162
		3	7/14	275
		4	8/6	199
B (sunflower)	2017	1	6/26	140
		2	7/23	121
	2018	1	6/20	134
		2	6/24	60
		3	7/15	114
		4	7/22	40
		5	8/31	130
C (sunflower)	2017	1	6/19	80
		2	6/30	80
	2018	1	6/20	140
		2	7/14	100
D (maize)	2017	1	6/13	150
		2	6/26	94
		3	7/6	50
		4	7/14	174
		5	8/6	120

Daily meteorological data, including air temperature, precipitation, relative humidity, wind speed, and sunshine duration, originated from the weather station at

480 the Shahaoqu experimental station. The soil moisture content for the four
481 experimental fields in 2017 and for field C in 2018 during the crop growing season
482 was measured every 7-10 days at the depths of 0-20, 20-40, 40-60, 60-80, 80-100 cm
483 by taking soil samples and oven drying. In 2018, in addition, the soil moisture content
484 at same depths was monitored daily using Hydra Probe Soil Sensors (Stevens Water
485 Monitoring System Inc., Portland, OR, USA) in field B except the oven drying method.
486 The Hydra Probe was calibrated using the intermittent manual measurements. In
487 2017, the groundwater depths were manually measured in all four experimental fields
488 about every 7-10 days. In 2018, the groundwater depth in fields B and C was
489 recorded at 30 min intervals using an HOBO Water Level Logger-U20 (Onset, Cape
490 Cod, MA, USA). The sensors of the soil moisture content and groundwater depth
491 were connected to data loggers and downloaded via wireless transmission. The crop
492 leaf area and crop height were manually measured every 7-12 days.

493 Undisturbed soil samples were collected in 5 cm high rings with a diameter of 5.5
494 cm from the five soil layers where the soil moisture were taken and used for textual
495 analysis, saturated soil moisture content, field capacity and soil bulk density. The soil
496 texture was analyzed with a laser particle size analyzer (Mastersizer 2000, Malvern
497 Instruments Ltd., United Kingdom). The American soil texture classification method
498 was used in this study. Finally, the soil samples were collected 7-10 days apart to
499 monitor the change of electrical conductivity (EC). The soil samples were mixed with
500 distilled water in a proportion of 1:5 to measure the electrical conductivity of the soil
501 water by a portable conductivity meter. It is assumed that 1 Ms cm^{-1} corresponds to

640 mg L^{-1} of total dissolved salts (Wallender and Tanji, 2011; Xue et al., 2018).

3.3 Model calibration and validation

The observed soil moisture contents, groundwater depths, crop heights, LAIs and salinity concentrations for field A with maize and sunflower fields B and C in 2017 were used for calibration and the sunflower data of fields B and C in 2018 and the maize data in field D in 2017 were used for validation. The initial θ_{fc} was based on the measured data (Table 2). The initial values of θ_s and θ_r were derived from the soil texture with the method of Ren et al. (2016) (Table2). The default values of EPIC for sunflower and maize were used as initial values for simulating crop growth (K_{cmax} and LAI_{mx} in Eq. S3, K_b in Eq. S4, H_{mx} in Eq. S7, PHU in Eq. S9,T_b in Eq. S10, ad in Eq. S12, T_0 and T_b in Eq. 16, RD_{mx} in Eq. S18). The initial value maximum crop coefficient (K_{cmax}) in Eq. S3 in Supplementary S1 for evapotranspiration calculation was taken from *Sau et al.*, (2004). The initial values of two groundwater parameters (a and b in Eq. 23) were based on Liu et al., (2019). The Brooks and Corey soil moisture characteristic parameters (φ_b, λ in Eq. 8) were obtained by fitting the outer envelope of the measure moisture content and water table data.

Statistical indicators were used to evaluate goodness of fit of the hydrological model for both calibration and validation (Ritter and Muñoz-Carpena, 2013). The statistical indicators included the root mean square error (RMSE) (Abrahart and See, 2000),

$$\mathrm{RMSE} = \sqrt{\frac{1}{N}\sum_{i=1}^{N}(P_i - O_i)^2} \qquad (30)$$

the mean relative error (MRE) (Dawson et al., 2006; Nash and Suscliff, 1970),

$$\mathrm{MRE} = \frac{1}{N}\sum_{i=1}^{N}\frac{(P_i - O_i)}{O_i} \times 100\% \quad (31)$$

the Nash-Sutcliffe efficiency coefficient (NSE) (Nash and Suscliff, 1970),

$$\mathrm{NSE} = 1 - \frac{\sum_{i=1}^{N}(P_i - O_i)^2}{\sum_{i=1}^{N}(O_i - \bar{O})^2} \quad (32)$$

and the determination coefficient (R^2) and regression coefficient (b) (Xu et al., 2015)

$$\mathrm{R}^2 = \left[\frac{\sum_{i=1}^{N}(O_i - \bar{O})(P_i - \bar{P})}{[\sum_{i=1}^{N}(O_i - \bar{O})]^{0.5}[\sum_{i=1}^{N}(P_i - \bar{P})]^{0.5}}\right]^2 \quad (33)$$

$$\mathrm{b} = \frac{\sum_{i=1}^{N} O_i \times P_i}{\sum_{i=1}^{N} O_{i=1}^2} \quad (34)$$

where N is the total number of observations; P_i and O_i are the i^{th} model predicted and observed values (i=1,2,3…N), respectively; $\bar{O}$ and $\bar{P}$ are the mean observed values and predicted values, respectively. The RMSE is used to evaluate the bias of the measured data and predicted data. The MRE can evaluate the credibility of the measured data. The NSE is usually used to evaluate the quality of the hydrological models. The R^2 is used to measure the fraction of the dependent variable total variation that can be explained by the independent variable. And the regression coefficient represents the influence of the independent variable on the dependent variable in the regression equation. The value of RMSE and MRE close to 0 indicates good model performance. The value of NSE ranges from -∞ to 1. NSE=1 means a perfect fit while the negative NSE value indicates the mean observed value is a better predictor than the simulated value (Moriasi et al., 2007). For b and R^2, the value closest to 1 indicates good model predictions.

543 3.4 Parameters sensitivity analysis

544 A sensitivity analysis was performed to determine how the input parameters
545 affected output of the models (Cloke et al., 2008; Cuo et al., 2011). Each parameter
546 was varied over a range of -30% to 30% to derive the corresponding impact on the
547 model output of soil moisture, groundwater depth, soil salinity, leaf area index and
548 actual evapotranspiration. The change in output values was plotted against the
549 change in input values.

550 **4. Results**

551 The 2017 and 2018 experimental data of the Shahaoqu farmers' fields in the
552 Hetao irrigation district (Fig.3) are presented first, followed by the calibration and
553 validation results of the CROP and VADOSE modules of EPICS model.

554 4.1 Results of the field experiment

555 4.1.1 Water input

556 The precipitation was 63 mm in 2017 (May 10 to September 30) and 108 mm in
557 2018 (June 1 to September 15). The precipitation from the greatest rainstorm was 26
558 mm on September 1, 2018 (Fig. 4). Irrigation provided most of the water for the crops.
559 Field A (maize) was irrigated four times with a total of 736 mm and field D (maize) was
560 irrigated five times for a total of 588 mm in 2017. Sunflower fields B and C were both
561 irrigated twice with a total water amount of 261mm and 160mm, respectively, in 2017.
562 In 2018, fields B and C were irrigated five and two times, respectively, with a total
563 water amount of 478mm and 240mm, respectively. The reference evapotranspiration
564 ranged from 1 mm d^{-1} to a maximum of 6.4 mm d^{-1} during crop growing period (Fig. 4).

The total reference evapotranspiration from May 10 to September 30, 2017 was 595 mm and 368 mm from June 1 to September 15, 2018. The reason was that there were more rainfall days in June, July and September in 2018 than in 2017, which increased the amount of water available for the evapotranspiration by the crop in 2018. In addition, the wind speed was high in May that increase the evapotranspiration was elevated. In the study of Ren et al. (2017) and Miao (et al. 2016), the mean ET_0 was over 6 mm per day on May. Hence, the ET_0 during the study period in 2017 was greater than in 2018.

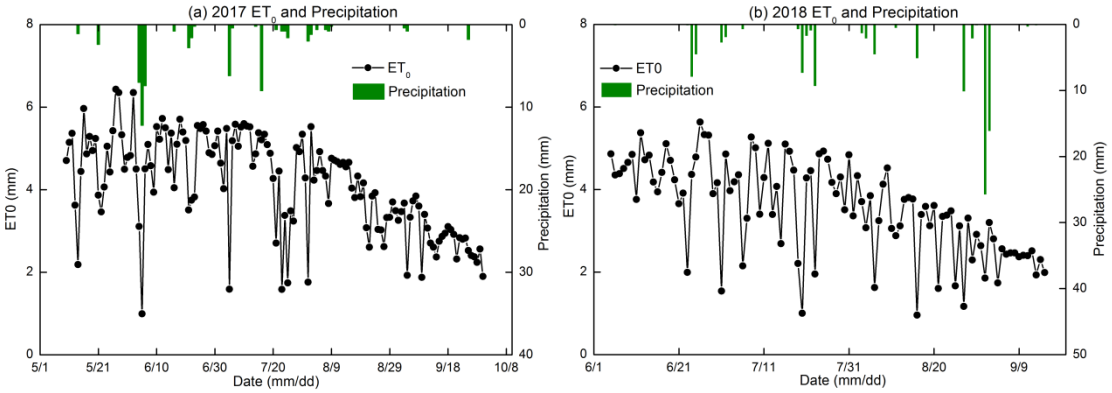

Figure 4. Reference evapotranspiration (ET_0) and precipitation during crop growth period in 2017 and 2018.

4.1.2 Soil physical properties

Based on the soil textural analysis in Table 2, the soils were classified as silt, silt loam and loamy sand. Bulk densities varied from 1.24 to 1.47 Mg m^{-3} with the greatest bulk densities in the 0-20 cm soil layer. There was generally more sand in the top 40 cm than below. The subsoil was heavier and had the greatest percentage of silt (Table 2). The moisture content at -33 kPa (0.33 bar) varied from 0.25 to 0.35 cm^3cm^{-3} and at 1.5 Mpa (wilting point at15 bar) ranged from 0.08 to 0.15 cm^3cm^{-3} (Table 2).

584 Table 2 Soil texture and bulk density of the experimental fields in Shahaoqu

Field	Soil depth (cm)	Sand(%)	Silt(%)	Clay(%)	Soil type	ρ(Mg m^{-3})	θ_{fc}(m^{3}m^{-3})	θ_r(m^{3}m^{-3})
A	0-20cm	26	62	13	Silt loam	1.44	0.31	0.1
	20-40cm	76	22	2	Loamy sand	1.24	0.32	0.07
	40-60cm	10	79	10	Silt loam	1.33	0.33	0.12
	60-100cm	6	79	15	Silt loam	1.35	0.34	0.14
							0.35	0.14
B	0-20cm	22	64	13	Silt loam	1.44	0.29	0.15
	20-40cm	16	73	11	Silt loam	1.24	0.26	0.13
	40-60cm	18	73	9	Silt loam	1.33	0.32	0.11
	60-80cm	8	77	16	Silt	1.35	0.34	0.14
	80-100cm	13	79	8	Silt loam		0.35	0.12
C	0-20cm	29	63	8	Silt loam	1.47	0.26	0.08
	20-40cm	37	56	6	Silt loam	1.33	0.25	0.08
	40-60cm	35	59	7	Silt loam	1.32	0.26	0.08
	60-80cm	14	74	12	Silt loam	1.38	0.31	0.12
	80-100cm	10	82	8	Silt	1.38	0.34	0.11
D	0-20cm	27	62	11	Silt loam	1.47	0.3	0.15
	20-40cm	5	80	15	Silt loam	1.33	0.27	0.14
	40-60cm	7	75	18	Silt loam	1.32	0.33	0.15
	60-100cm	10	81	9	Silt	1.38	0.34	0.12
							0.31	0.14

585

586 4.1.3 Soil moisture content

587 Moisture content, rainfall and irrigation amounts are depicted for the five layers
588 and the four fields in 2017 and two fields in 2018 in Fig. 5. Blue closed spheres
589 indicate that the moisture content was determined on cored soil samples (Figs. 5a, b,
590 c, e, f) and close-spaced spheres when the hydra probe was used (Fig. 5d). The
591 moisture contents were near saturation when irrigation water was added and
592 subsequently decreased due to crop transpiration and soil evaporation (Fig. 5). In all
593 cases, the moisture contents during the main growing period remained above the

moisture content at -33 kPa that ranged from 0.25 cm^3cm^{-3} to 0.34 cm^3cm^{-3} for the 60-80 cm depth (Table 2, Fig.5). Only after the last irrigation and during harvest of the crop did the moisture content in the top 0-40 cm for maize and 0-60 cm for sunflower decrease below the moisture content at -33 kPa. During the growing season, the variation of moisture content was greater in the top 60 cm with the majority of the roots than in the lower depths where, after the first irrigation, it remained nearly constant close to saturation.

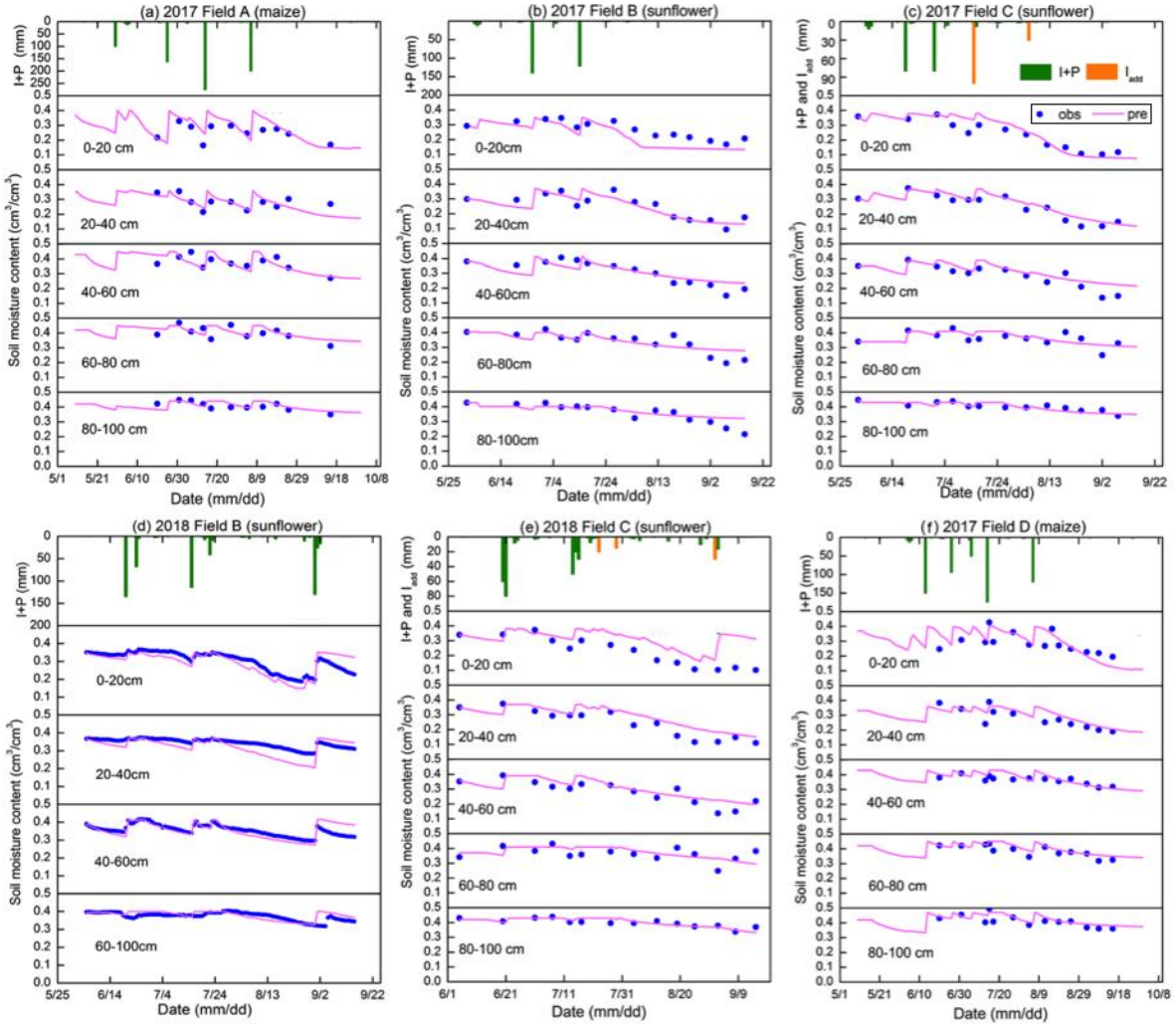

Figure 5. Observed (blue dots) and simulated soil moisture content of the Shahaoqu experimental fields during model calibration (a,b,c) and validation (d,e,f)

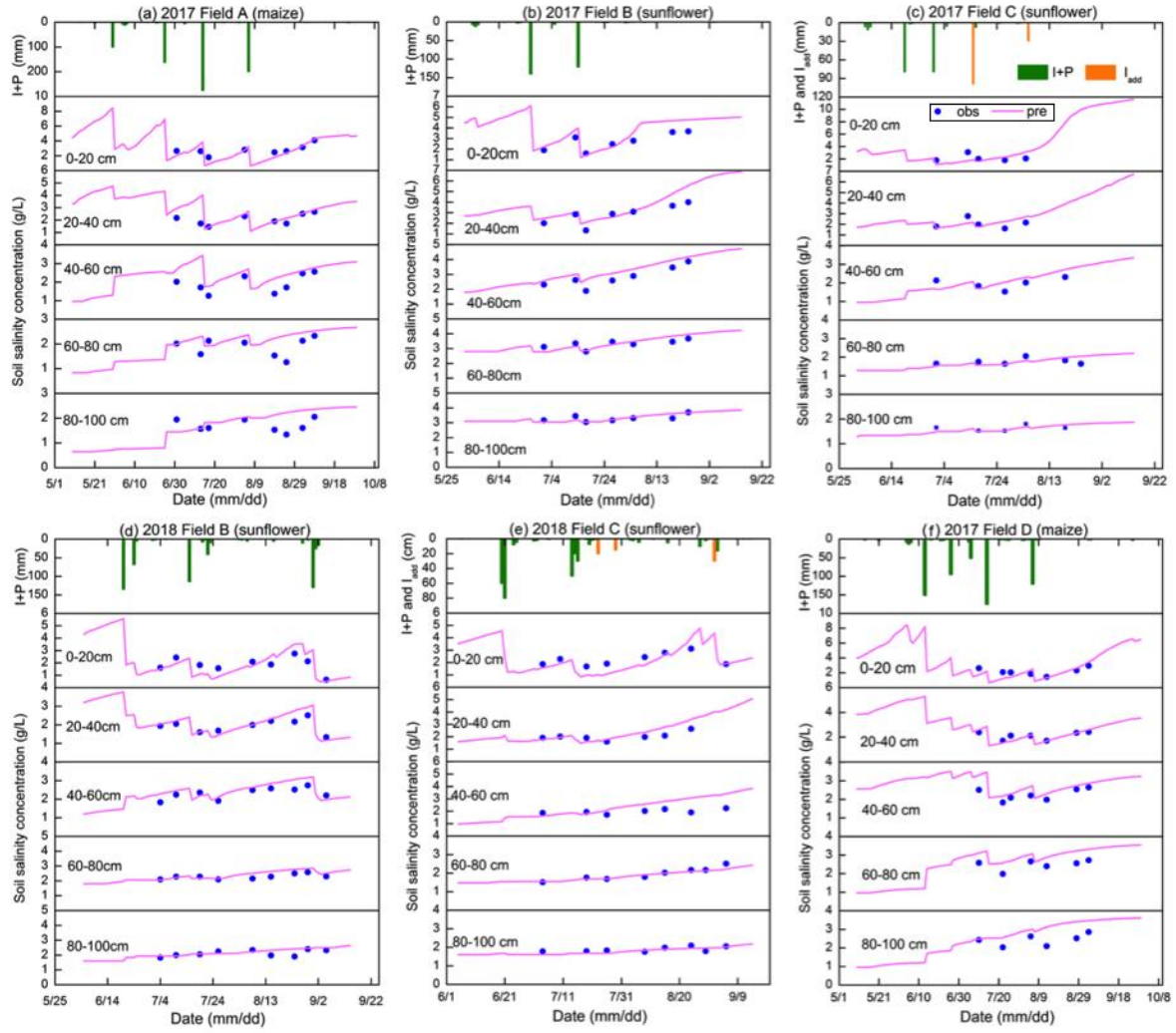

Figure 6. Observed (blue dots) and simulated soil salinity concentration of the experimental fields in Shahaoqu during model calibration (a,b,c) and validation (d,e,f).

4.1.4 Salinity

Overall the salt concentration is greatest at the surface and increases at all depths during the growing season. Sunflower is more salt tolerant than maize and the overall salt concentration was greater in the sunflower fields (Fig. 6) at comparable times of the crop development for field B but not for field C. Comparing the salt concentration and soil moisture patterns (Fig.5), we note that they behave similarly but opposite to each other (Fig. 6). The soil salinity concentration was decreasing

during an irrigation event due to dilution and then gradually increasing partly due to evaporation of the water. Some of the soil salt was transported to the layers below during irrigation and some salt was moving upward with the evaporation from the surface. As expected, after the harvest, the autumn irrigation decreased the salt concentration from fall 2017 to spring 2018.

4.1.5 Groundwater observations

The variation in groundwater depth during the growing season was very similar for both years and in all fields. The groundwater depth for all fields was between 50 and 100 cm from the surface after an irrigation event and then decreased to around 150 cm before the next irrigation or rainfall (Fig.7). Only after the last irrigation in August 2017 did the water table decrease to below 250 cm and to around 200 cm in 2018. Field D followed the same pattern but the groundwater was more down from the surface. In several instances, the groundwater table increased without an irrigation or rainfall event in sunflower field C (Fig. 7c and 7e). This was likely related to an irrigation event either from an irrigation in nearby field that affected the overall water table or an accidental irrigation that was not properly documented. We estimated the amount of irrigation water based on the change in moisture content in the soil profile (orange bars in Fig. 7c and 7e). Finally, there was a notable rise in the water table of an mean 375mm “autumn irrigation” after harvest between the end of 2017 (Figs. 7 a, b, c) and the beginning of 2018 (Figs. 7 d, e, f), which is a common practice in the Jiefangzha irrigation district to leach the salt that has accumulated in the profile during the growing periods.

Note that in Fig. 7, after an irrigation event, the groundwater depth was between 50-80 cm while the whole profile was saturated (Fig. 5). This is directly related to the bubbling pressure of the water. After the irrigation event stopped, the water table was likely at the surface but then immediately decreased because a small amount of evaporated water will bring the water table down to a depth of approximately equal to the bubbling pressure, φ_b, in Eq. 5. The bubbling pressures are listed in Table 3.

4.1.6 LAI and plant height

Plant height and LAI followed the typical growth curve that started slowly to rise in the beginning, accelerated during the vegetative stage and then became constant during the seed setting and ripening stages (Fig. 8). In the maturing stage, the leaf area index decreased.

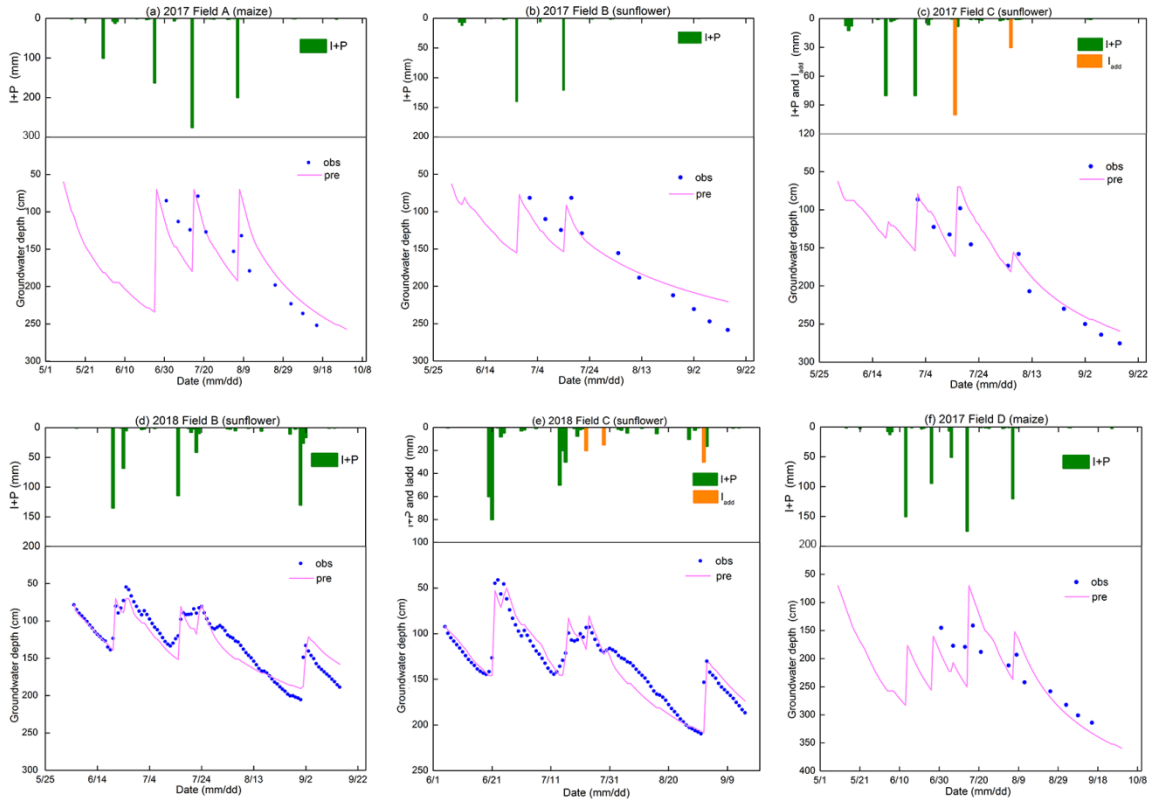

Figure 7. Observed (blue dots) and simulated groundwater depth of the experimental fields in Shahaoqu during model calibration (a, b, c) and validation (d, e, f)

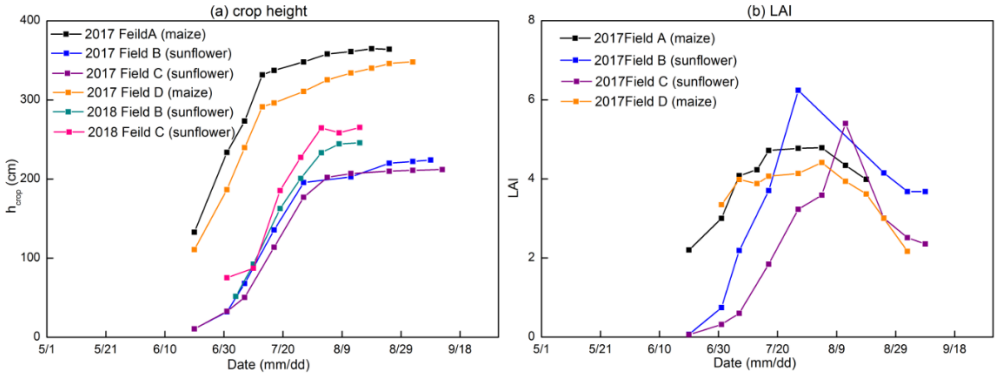

Figure 8. Observed crop height (a) and leaf area index (b) of the experimental field in Shahaoqu in 2017 and 2018.

4.2 Soil Characteristic curve and drainable porosity

To simulate the soil moisture content and to derive drainable porosity as a function of water table depth, the soil moisture characteristic curves were derived by plotting the observed soil moisture content in 2017 and 2018 versus the height above the water table to the soil surface for the five soil layers in Fig. 9. The Brooks-Corey equation (Brooks and Corey, 1964) was fitted through outer envelope of the points. The parameters of the Brooks-Corey equation were adjusted through a trial and error to obtain the best fit (Table 3a). In Fig. 9, points on the left side of the soil moisture characteristic curve (moisture content smaller than the field capacity) were due to water removal at times when evaporative demand was greater than the upward water flux. Under these conditions the conductivity is limiting in the soil and there is no relationship between groundwater depth and matric potential. Since we take the water table depth as proxy for matric potential, these points are omitted when drawing the soil characteristic curve. The few points at the right of the soil moisture characteristic curve indicate the soil moisture was greater than field capacity and

matric potential and groundwater were not yet at equilibrium after an irrigation event.

The fitted parameter values are consistent. Field A had a greater bubbling pressure and moisture content at -33 kPa than the other fields indicating that this field had more clay. This was confirmed by the data in Table 2. For fields B, C and D, the bubbling pressure was greater at the 60-80 cm depth or the 80 -100 cm depth, which was also in accordance with the data in Table 2.

Table 3a Calibrated soil hydraulic parameters in the Brooks and Corey soil moisture characteristic curve.

Field	Parameter	0-20cm	20-40cm	40-60cm	60-80cm	80-100cm
A	θ_s	0.4	0.36	0.43	0.45	0.47
	φ_b	80	100	90	70	50
	λ	0.18	0.21	0.22	0.18	0.15
B	θ_s	0.35	0.37	0.41	0.4	0.4
	φ_b	50	55	33	60	55
	λ	0.14	0.11	0.16	0.2	0.2
C	θ_s	0.38	0.37	0.39	0.71	0.43
	φ_b	55	50	40	60	40
	λ	0.26	0.24	0.2	0.18	0.13
D	θ_s	0.4	0.36	0.45	0.45	0.44
	φ_b	50	40	55	50	50
	λ	0.21	0.2	0.3	0.17	0.15

Note: θ_s is the soil moisture at saturation (cm^3cm^{-3}), φ_b is bubbling pressure (cm), λ is the pore size distribution index.

Table 3b Calibrated groundwater parameters

Field\parameters	A	B	C	D
a	70	75	110	70
b	0.02	0.025	0.022	0.015

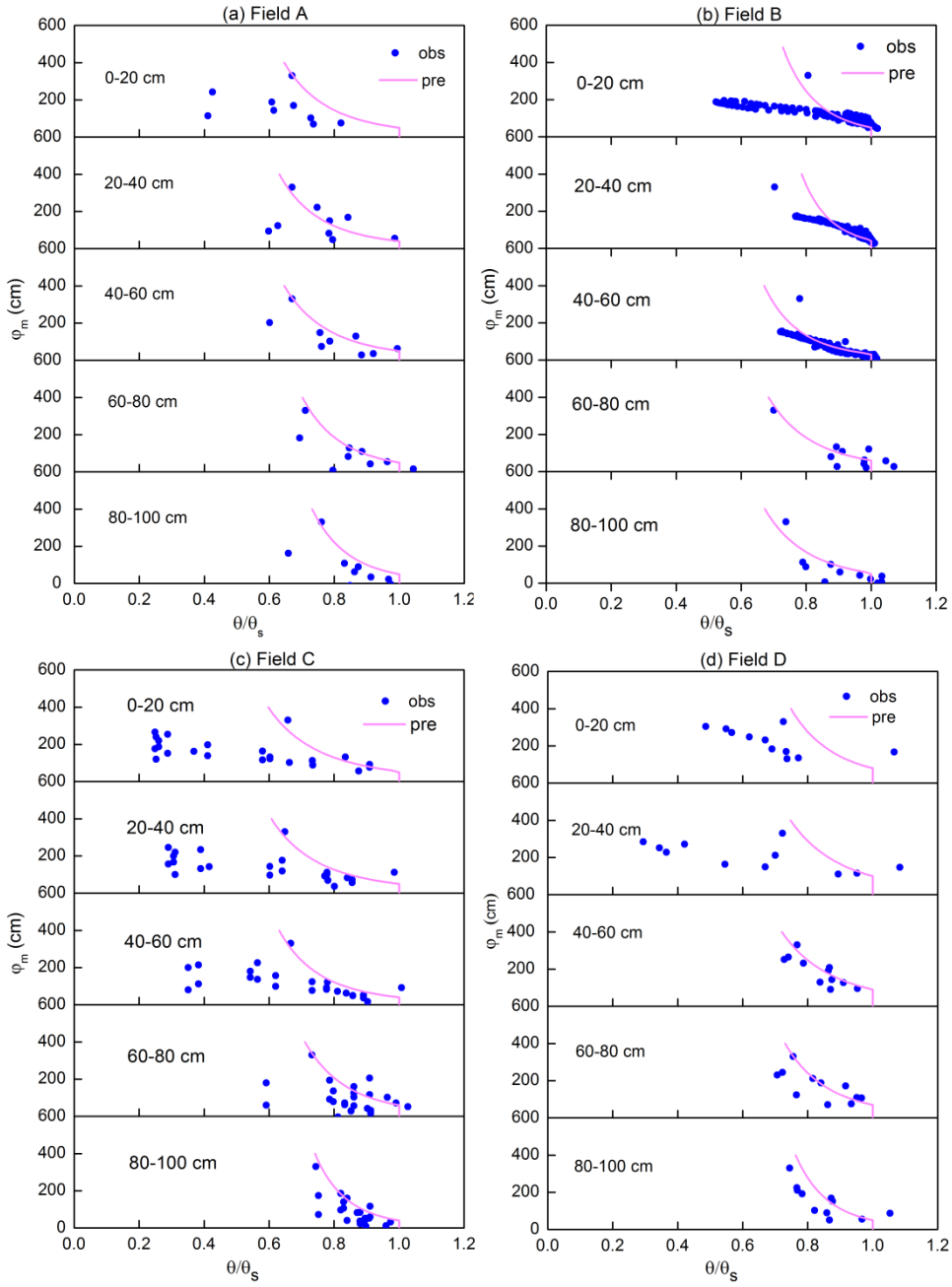

Figure 9. Soil moisture characteristic curves of five soil layers in the experimental fields. The pink line is the fit with the Brooks-Corey equation.

4.3 Parameters sensitivity analysis

The results of sensitivity analysis of the 15 input parameters on 5 output parameters are shown in Fig. 10. The evaluated output parameters are soil moisture content, groundwater depth, soil salinity concentration, field evapotranspiration, and crop leaf

689 area index (LAI). Steeper lines indicate a greater sensitivity of the parameter.

690 The results of the sensitivity analysis show that moisture content predictions (Fig
691 10a) are the most sensitive to the input value of the saturated moisture content (θ_s).
692 None of the other parameters are very sensitive. This includes the shape parameters
693 for the soil characteristic curve, bubbling pressure φ_b, and the exponent λ. The input
694 parameter with the most sensitivity for *groundwater depth (*Fig. 10b), is the saturated
695 moisture content as well. Other less sensitive parameters are the exponent *b* and
696 constant *a* in Eq. 23 in predicting the upward flux and the bubbling pressure, φ_b, of the
697 soil moisture characteristic curve (Eq. 8a). Likewise, in case of the *salinity* predictions
698 (Fig. 10c), the saturated moisture content gives the greatest relative change in salt
699 content. Less sensitive, but still important, are the field capacity, θ_{fc}, the bubbling
700 pressure, $\varphi_{b,}$ and the exponent λ of the soil characteristic curve (Eq. 8a) and *b* in Eq.
701 23. The sensitive parameters for the *leaf area index (LAI)* (Fig 10d) are the maximum
702 potential leaf area index, LAI_{mx}, and fraction of growing season when leaf area
703 declines (*DLAI*) followed by total potential heat units required for crop maturation
704 (*PHU*). Finally, for the evapotranspiration (Fig 10e), the saturated soil moisture
705 content is the most sensitive parameter, and other less sensitive parameters are the
706 exponent *b* and field capacity.

707 Thus, the model output is most sensitive to the input parameters that define the
708 soil hydraulic properties, groundwater flux and crop growth. As expected, since the
709 soil remains near field capacity, the parameters that relate to the reduction of
710 evaporation when the soil dries out are insensitive. When used in the simulation

711 practices, the model needs to be calibrated and verified to avoid high error from

712 parameters uncertainty.

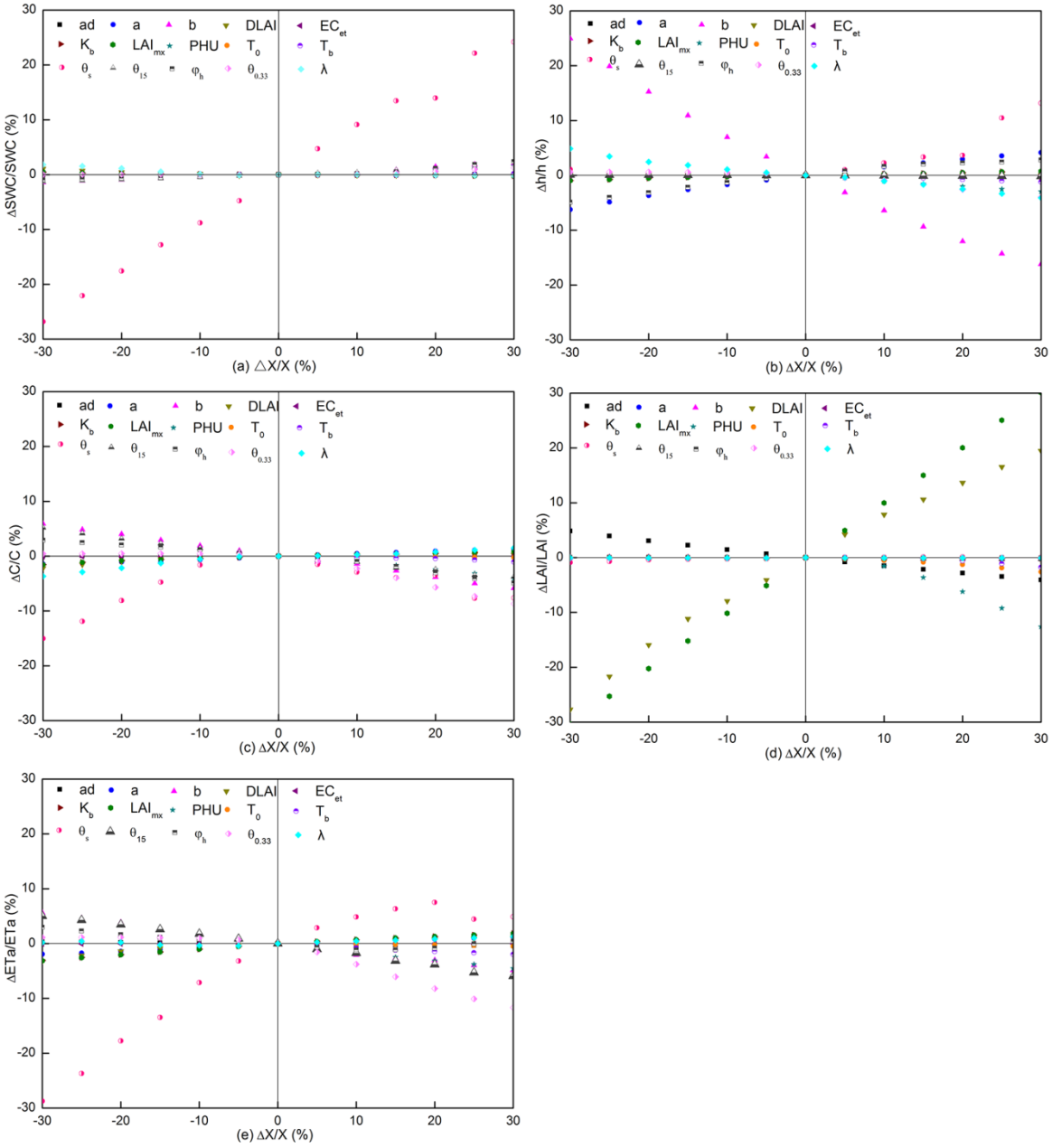

713

714 Figure 10. Parameters sensitivity analysis for (a) soil moisture content, (b)

715 groundwater depth, (c) salt salinity concentration, (d) LAI, (e) ET

716

717 4.4 Model calibration and validation with field data

718 The model parameters were calibrated and validated using the observed moisture

719 content, groundwater depth, plant height, leaf area index and the calculated

720 evapotranspiration. The data of sunflower fields B and C and maize field A were
721 collected and used for calibration. Since farmers did not grow maize in 2018, the
722 2017 data of maize field D, together with sunflower fields B and C in 2018 were used
723 for validation. The optimal parameter set was determined using graphical similarity
724 between observed and predicted results together with near optimum performance of
725 the statistical indicators while keeping all values within physical acceptable ranges.

726 As a way of reducing the number of parameters that needed to be calibrated, we
727 initially selected one to three most sensitive parameters for each of the observed time
728 series, starting with evapotranspiration (including *LAI* and crop height) followed by
729 moisture content, groundwater depth, and salt content in the soil. This cycle was
730 repeated several times until changes became small. The last stage of the calibration
731 consisted of fine-tuning the remaining least sensitive parameters.

732 To calibrate the parameters in the CROP module, we calculated
733 evapotranspiration during the crop growth period with the observed soil moisture
734 content and groundwater depth by the soil water balance method. In addition, we
735 used the observed *LAI* measurements in 2017 and plant height in both 2017 and
736 2018. *LAI* was not measured in 2018. The *DLAI*, LAI_{mx} and H_{mx} in the crop module
737 were adjusted to fit the observed *LAI* and crop height values. In addition, we fitted the
738 θ_{fc} moisture content to obtain a good fit of the evapotranspiration. The saturated
739 moisture content values were not adjusted since they were already determined for
740 fitting the soil characteristic curve. The exponent *b* and constant *a* in Eq. 23 were
741 adjusted to fit the observed soil moisture content and groundwater depth.

742 4.4.1 Evapotranspiration, crop height and leaf area index

743 The predicted evapotranspiration and that calculated from the mass balance
744 show a good agreement with Nash Sutcliff values ranging from 0.96-0.89 during
745 calibration and validation (Fig. 11 and Table 4). The calibrated predictions of plant
746 height fitted the observed values well during calibration and validation with Nash
747 Sutcliff values ranging from 0.77-0.96 for the individual fields (Table 4) and over 90%
748 when the data was pooled for the fields during calibration and validation (Fig.12). LAI
749 was not measured in 2018. During calibration, Nash Sutcliff predicted LAI values
750 were good for sunflower but not as good for maize but the coefficient of determination
751 and slope in the regression were acceptable (Table 4, Fig. 13). In addition, the overall
752 trend was predicted reasonably well (Fig. 13b).

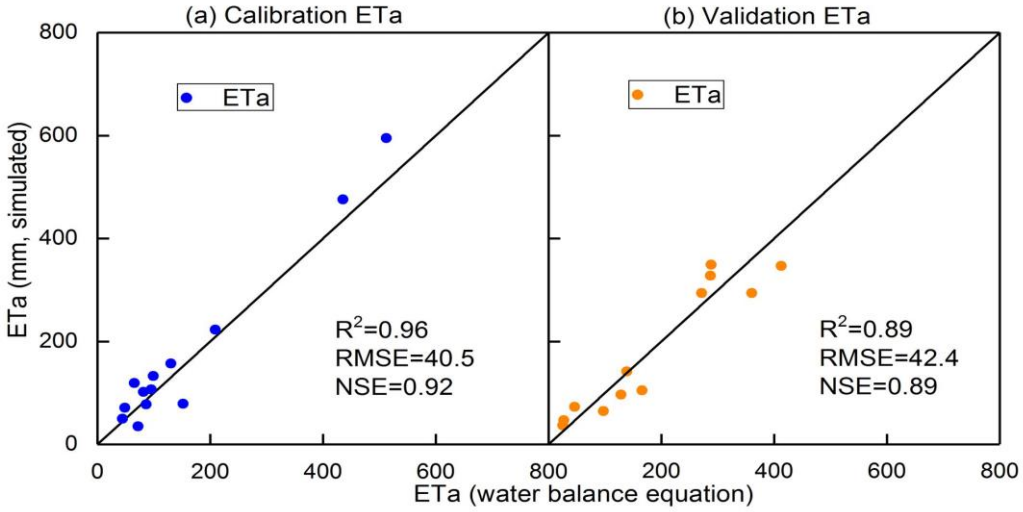

753

754 Figure 11. Comparison of predicted and observed actual evapotranspiration: a)
755 Calibration and b) Validation

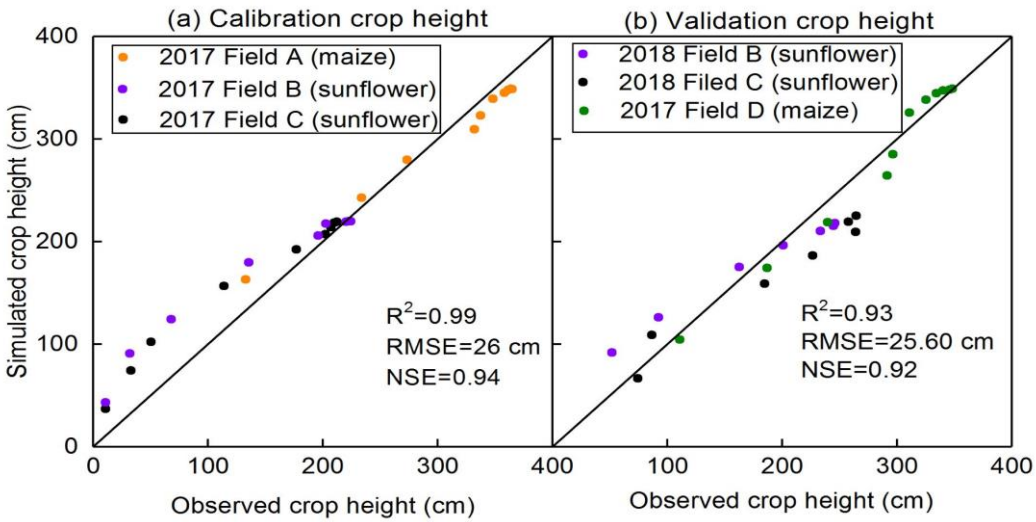

Figure 12. Comparison of predicted and observed crop height: a) Calibration and b) Validation

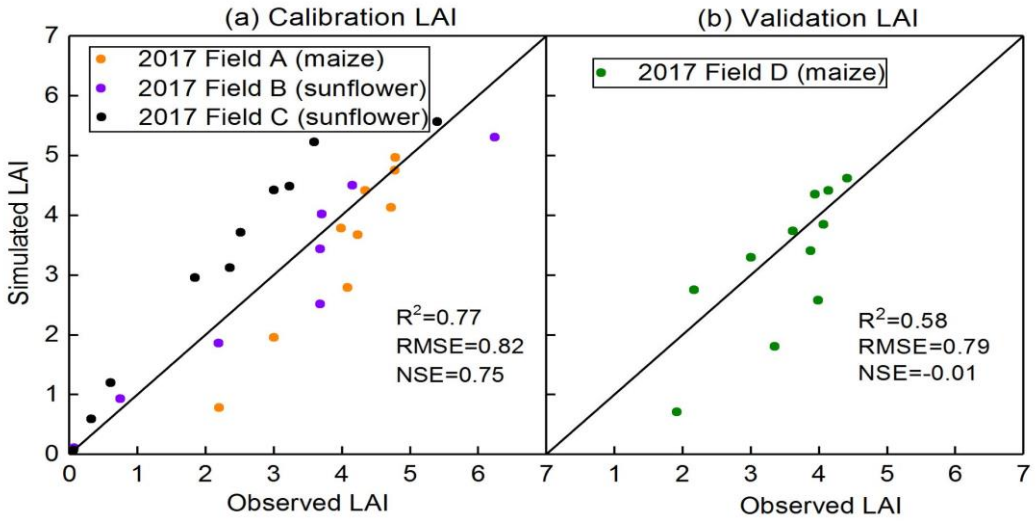

Figure 13. Comparison of predicted and observed LAI: a) Calibration and b) validation

769 Table 4 Model error statistics for calibration and validation of model in 2017 and 2018
770 (Mean relative error, MRE; root mean square error, RMSE; Regression slope;
771 Coefficient of determination, R^2; Regression coefficient, slope).

Process	Field	Variable	MRE (%)	RMSE ($cm^3cm^{-3}cm$ or gL^{-1}or mm)	NSE	R^2	Regression coefficientslope
Calibration	2017 Field A (maize)	SWC (0-1m)	2.9	0.04	0.8	0.56	1.01
		GWD	4.5	33.8	0.64	0.64	0.97
		LAI	-17.4	0.78	0.11	0.92	0.89
		hcrop	0.04	16.2	0.95	0 .99	0.97
		C (0-1m)	13.9	0.5	*	0.49	1.07
	2017 Field B (sunflower)	SWC (0-1m)	-1.2	0.04	0.71	0.74	0.97
		GWD	6.0	22.9	0.86	0.98	0.96
		LAI	4.7	0.58	0.9	0.92	0.91
		hcrop	6.8	33.5	0.83	0.96	1.1
		C (0-1m)	11.0	0.55	*	0.7	1.1
	2017 Field C (sunflower)	SWC (0-1m)	8.5	0.04	0.88	0.9	1.05
		GWD	-7.3	19.1	0.91	0.94	0.94
		LAI	48.6	1.0	0.59	0.93	1.29
		hcrop	5.42	27.4	0.88	0.98	1.07
		C (0-1m)	-1.6	0.52	*	0.08	0.94
		ETa	12.2	40.5	0.92	0.96	1.11
Validation	2018 Field B (sunflower)	SWC (0-1m)	-2.3	0.03	0.43	0.68	0.98
		GWD	4.86	16.1	0.83	0.84	1.01
		hcrop	12.5	26.9	0.86	0.99	0.95
		C (0-1m)	4.0	0.35	*	0.72	1.06
	2018 Field C (sunflower)	SWC (0-1m)	17.3	0.06	0.64	0.72	1.04
		GWD	2.1	13.8	0.86	0.87	1.01
		hcrop	-10.3	36.4	0.77	0.97	0.84
		C (0-1m)	0.51	0.33	*	0.73	1.02
	2017 Field D (maize)	SWC (0-1m)	6.1	0.04	0.68	0.77	1.05
		GWD	0.64	39.1	0.52	0.71	1.01
		LAI	-10.7	0.79	-0.02	0.58	0.93
		hcrop	-1.7	13.6	0.96	0.98	1
		C (0-1m)	9.8	0.51	*	0.54	1.11
		ETa	8.0	42.4	0.89	0.89	0.95

772 Note: * Relative bias was over 5% invalidating the calculation of NSE. SWC is the soil
773 moisture content, GWD is the groundwater depth, LAI is the leaf area index, hcrop is
774 the height of the crop, C is the soil salinity concentration, ETa is the actual
775 evapotranspiration.

776 4.4.2 Soil moisture and groundwater depth

777 Next, the moisture contents and groundwater table were fitted with the parameters in
778 the Vadose model without changing the parameters in the CROP module. Saturated
779 moisture content was the most sensitive parameter for calibrating the moisture
780 content (Fig.10a). Since this value was already determined a priori from the soil
781 characteristic curve (Table 3a), we could not use other parameters to obtain a better
782 fit since none were sensitive (Fig.10a). Therefore, we calibrated the groundwater
783 parameters (i.e., *a* and *b* parameters (Eq. 23)) together with the moisture content to
784 obtain the best fit for both. The fitted *a* and *b* values are listed in Table 3b. The fitted
785 parameters between the four experimental fields were similar but not the same. This
786 can be expected in river plains where soils can vary over short distances.

787 Overall, the moisture contents were predicted well during calibration and
788 validation (Figs. 5, 14 and Table 4) with the exception of field B during validation
789 (Table 4) with a NSE of 0.43. The moisture contents were predicted most accurately
790 in the layers from 40-100cm where the soil moistures were at field capacity during
791 most of the growing season (Fig. 14). In the top 40 cm, the predicted soil moisture
792 content deviated from observed moisture contents, especially at the dryer end (Fig. 5
793 and 14). Unlike at deeper depths, evapotranspiration determined the moisture
794 contents at shallow depths. Prediction of evapotranspiration introduced additional
795 uncertainties such as the distribution of the root system. This uncertainty is also likely
796 the reason why the 2018 moisture contents during the validation are acceptable but
797 not predicted as well as in 2017.

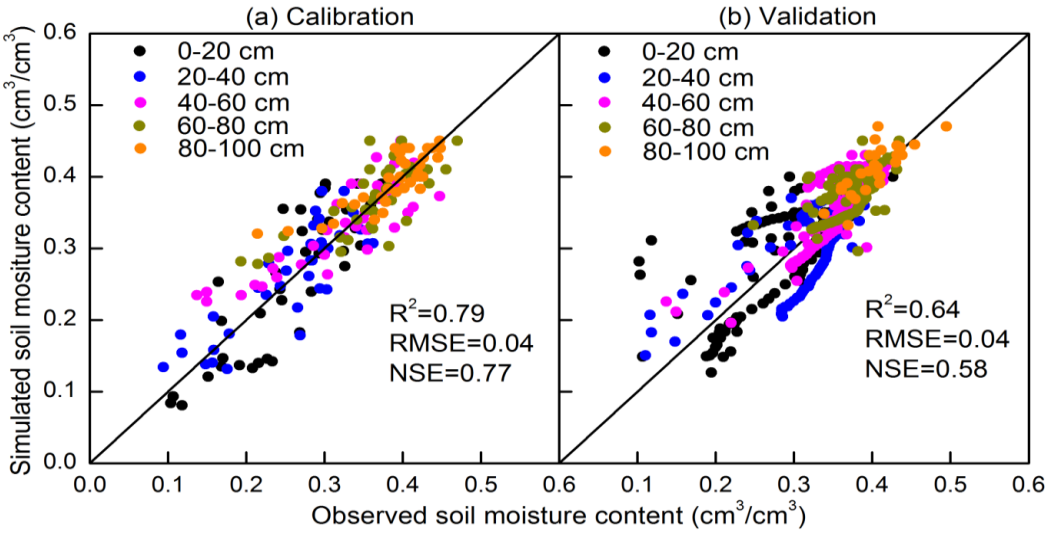

Figure 14. Comparison of predicted and observed soil moisture content: a) calibration and b) validation

The predicted and observed groundwater depths are in good agreement during both calibration and validation (Figs 7, 15). The MRE values were within $\pm 10\%$ and the NSE values ranged from 0.52 for field D during validation to 0.91 in field C during calibration where some of the recharge events were estimated (Table 4).

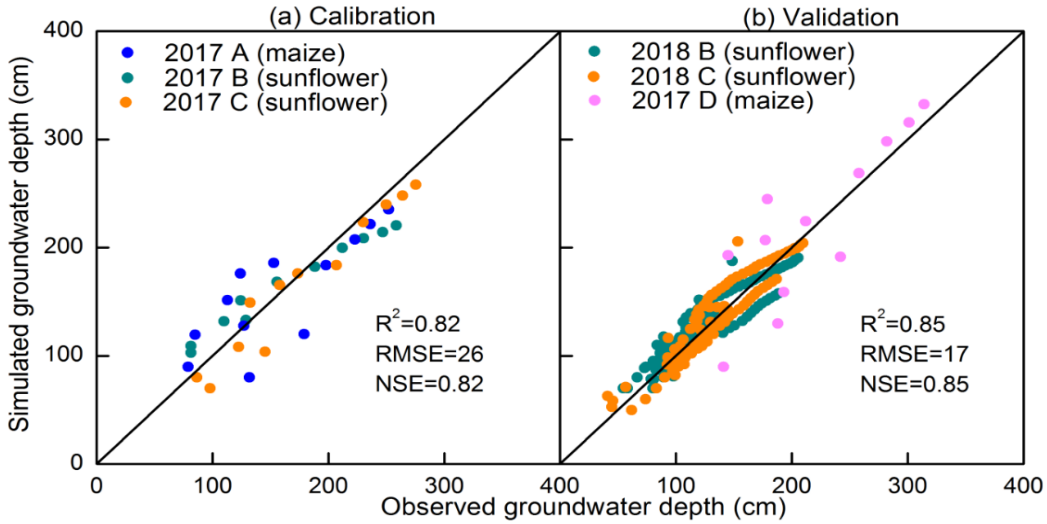

Figure 15. Comparison of predicted and observed groundwater depth a) calibration and b) validation.

4.4.3 Soil salinity

The only parameter that could be adjusted each year for calibration of the salt concentrations was the initial salt concentration. The predicted salt concentrations in the top layers decreased after an irrigation event similar to the limited observed values (Figs. 6). Despite that the salt concentration fitted visually reasonably well as shown in Figures 6 and 16, there was a bias of 8% in the data and consequently the Nash Sutcliff efficiency could not be applied (Table 4) (Ritter and Muñoz-Carpena, 2013). Similarly to the moisture contents, the salt concentrations in the layers below 40 cm were predicted more accurately than the layers above the 40 cm. More data should be collected during the whole year on the salt concentrations in the soil in order to accurately predict the salt concentrations.

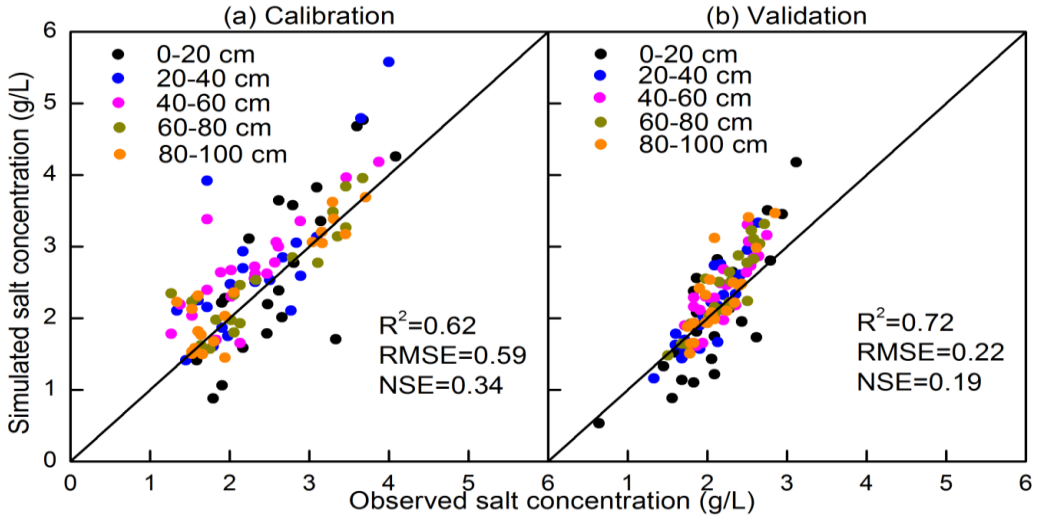

Figure 16. Comparison of predicted and observed salt concentration during calibration (a) and validation (b)

5. Discussion

The EPICS model is a surrogate model that can be applied in areas with shallow groundwater. It can simulate the soil moisture content and salt concentration for layers in the soil, the groundwater depth, upward movement of water from

827 groundwater, evapotranspiration, and plant growth.

828 The model is different from traditional models that are based on Richards
829 equation; instead of calculating the fluxes first, in the EPICS model, the groundwater
830 depth is calculated first based either on the amount of water removed by
831 evapotranspiration on days without rain or irrigation or recharge to groundwater on
832 the other days. Subsequently, when the groundwater is sufficiently shallow and the
833 potential upward flux from the groundwater is greater than the evaporative demand,
834 the moisture contents are adjusted so that soil moisture and groundwater depth are in
835 equilibrium (i.e., field capacity). In this case, the matric potential is equal to the height
836 above the water table and the moisture contents can be found with the soil
837 characteristic curve. When the upward flux is less than the evaporative demand of the
838 atmosphere and crop, the difference between the upward moisture content is
839 determined by first decreasing the moisture content below the field capacity. The flux
840 of water in the soil is then calculated based on the changes in water content. The
841 advantage is fewer input parameters needed when compared with other numerical
842 models (Šimůnek et al., 1996; Dam et al., 1997). For example, the hydraulic
843 conductivity is not used in EPICS.

844 Although the uncertainties of field experimental observations and input data of
845 the model affected the accuracy of simulation results, EPICS compares well with
846 other models. Xu et al. (2015) tested the SWAP-EPIC for two lysimeters grown with
847 maize on the same experimental farm in the Hetao irrigation district where our
848 experiment was carried out. The SWAP model solves the Richards' Equation

849 numerically with an implicit backward scheme and is combined by Xu et al. (2015)
850 with the EPIC model. The accuracy of our simulation results, despite the difference in
851 complexity, are very similar. The moisture contents were simulated slightly better with
852 EPICS, the groundwater depth was nearly the same, and the LAI values were
853 predicted more accurately in the SWAP-EPIC model. Xue et al. (2015) did not
854 simulate the salt content of the soil. Compared to less data and computational
855 intensive models that are applied in the Yellow River, the soil moisture content were
856 simulated more accurately by EPICS than in the North China Plain with 30 m deep
857 groundwater by surrogate models of Kendy et al. (2003) and Yang et al. (2015 a,b)
858 and in the Hetao irrigation district by Gao et al. (2017b) and Xue et al. (2018) during
859 the crop growth period.

860 To obtain more accurate results in the future, the upward capillary flux from
861 groundwater needs to be improved. The salinity of irrigation source water also needs
862 to be measured, especially for the areas irrigated by groundwater or the
863 hydrologically closed basins. In addition, the evapotranspiration measured
864 independently, using Eddy covariance (Zhang et al., 2012; Armstrong et al., 2008)
865 and Bowen ratio-energy balance method (Zhang et al., 2007) should be further used
866 to test performance of the model in the future study.

867 The limitation of the EPICS model is it can only be applied in areas where
868 groundwater is generally less than 3.3 m deep. When the groundwater is deeper than
869 3.3 m, the field capacity of the surface soil is determined by the moisture content
870 when the hydraulic conductivity becomes limiting and not by the depth of the

groundwater.

Overall, the present model has the advantage that it greatly simplifies the calculation of the moisture content, groundwater depth and salt content and despite that, gives results similar to or better than other models applied in the Yellow river basin.

6. Conclusions

A novel surrogate field hydrological model called *Evaluation of the Performance of Irrigated Crops and Soils* (EPICS) was developed for irrigated areas with shallow groundwater. The model was tested with two years experimental data collected by us for sunflower and one year of maize on replicated fields in the Hetao irrigation district, a typical arid to semi-arid irrigation district with a shallow aquifer. The EPICS model uses the soil moisture characteristic curve, upward capillary flux, and groundwater depth to derive the drainable porosity and predict the soil moisture contents and salinity. The evaporative flux is calculated with equations in EPIC (Environmental Policy Integrated Climate) and root distribution equation.

The simulation results show that the EPICS model can predict the soil moisture content and salt concentration in different soil layers, groundwater depth, and crop growth on a daily time step with acceptable accuracy during calibration and validation. The saturated soil moisture content is the most sensitive parameter for soil moisture content, salt concentration, and ET in our model.

In the future, the model should be tested in other areas with shallow groundwater that can be found in surface irrigated sites and in humid climates in river plains. Once

fully tested, the EPICS model can be used for optimizing water use at the local scale but, more importantly, on a watershed scale in closed basins where every drop of water counts.

Data availability: The observed data used in this study are not publicly accessible. These data have been collected by personnel of the College of Water Resources and Civil Engineering, China Agricultural University, with funds from various cooperative sources. Anyone who would like to use these data, should contact Zhongyi Liu, Xianghao Wang and Zailin Huo to obtain permission.

Author contributions: LZ and XW collected the data. ZL, ZH, CW, GH, XX and TS contributed to the development of the model. The simulations with the model were done by ZL, ZH and TS. Preparation and revision of the paper were done by ZL under the supervision of TS and ZH.

Competing interests: The authors declare that they have no conflicts of interest.

Acknowledgements: Peggy Stevens helped greatly with polishing the English. We thank Xianghao Wang and Limin Zhang and the technicians in the Shahaoqu experimental station who helped in collecting data.

Financial support: This study has been supported by National Key Research and Development Program of China (2017YFC0403301, 2016YFC0400107) and the National Natural Science Foundation of China (No. 51639009, 51679236).

References

Abrahart, R.J and See, L.: Comparing neural network and autoregressive moving average techniques for the provision of continuous river flow forecasts in two contrasting catchments. Hydro. Processes, 14: 2157-2172. http: // doi.org/10.1002/1099-1085(20000815/30)14:11/12<2157::AID-HYP57>3.0.CO;2 -S. 2000.

Allen, R.G., Pereira, L.S., Raes, D., and Smith, M.: Crop evapotranspiration. Guidelines for computing crop water requirements-FAO Irrigation and Drainage Paper 56, FAO, Rome. 1998

Armstrong, R.N., Pomeroy, J. W., Martz, L.W.: Evaluation of three evaporation estimation methods in a Canadian prairie landscape. Hydrol. Process, 22(5): 2801-2815. https:// doi.org/ 10.1002/hyp.7054. 2008.

Asher, M.J., Croke, B.F.W., Jakeman, A.J. and Peeters, L.J.M.: A review of surrogate models and their application to groundwater modeling. Water Resour Res, 51:5957-5973. http://doi.wiley.com/10.1002/2015 WR016967. 2015.Blanning, R. W., The construction and implementation of metamodels, Simulation, 24(6): 177-184. https:// doi.org/10.1177/003754977502400606.1975.

Babajimopoulos, C., Panoras, A., Georgoussis, H., Arampatzis, G., Hatzigiannakis, E., Papamichail, D.: Contribution to irrigation from shallow water table under field conditions. Agr. Water Manage. 92:2015-210. https://doi.org/ 10.1016/j.agwat.2007.05.009

Brooks, R.H., and Corey, A.T.: Hydraulic properties of porous media, Hydrology Paper 3. Colorado State University. Fort Collins, Colorado, 37pp, 1964.

Blanning, R.W.: Construction and Implementation of Metamodels. Simulation, 24(6):177-184. https:// doi.org/ 10.1177/003754977502400606. 1975.

Chen, C., Wang, E., and Yu, Q.: Modelling the effects of climate variability and water management on crop water productivity and water balance in the North China Plain. Agr. Water Manage., 97:1175-1184. https:// doi.org/10.1016/j.agwat.2008.11.012. 2010.

Chen, S., Huo, Z., Xu, X., Huang, G.: A conceptual agricultural water productivity model considering under field capacity soil water redistribution applicable for arid and semi-arid areas with deep groundwater, Agr Water Manage, 213, 309-323. https:// doi.org/10.1016/j.agwat.2018.10.024. 2019.

949 Cloke, H., Pappenberger, F., Renaud, J.: Multi-Method Global Sensitivity Analysis
950 (MMGSA) for modelling floodplain hydrological processes. Hydrol Process, 22(1):
951 1660-1674. https:// doi.org/ 10.1002/hyp.6734. 2008.

952 Cuo, L., Giambelluca, T., Ziegler, A.: Lumped parameter sensitivity analysis of a
953 distributed hydrological model within tropical and temperate catchments. Hydrol
954 Process, 25(15): 2405-2421. http://doi.org/ 10.1002/hyp.8017. 2011.

955 Dam, JC. Van., Huygen, J, Wesseling, JG, Feddes, RA., Kabat, P.,Walsum, PEV.
956 Van.,Groenendijk, P., Diepen.: Theory of SWAP version 2.0. Simulation of water
957 flow, solute transport and plant growth in the soil-water-atmosphere-plant
958 environment. Report 71, Deparment Water Resources, Wageningen Agricultural
959 University. Technical document 45, DLO Winand Staring Centre,
960 Wageningen,152pp, 1997.

961 Dawson, C.W., Abrahart, R.J., Shamseldin, A.Y., Wilby, R.L.: Flood estimation at
962 ungauged sites using artificial neural networks. J Hydrol.319: 391-409.
963 http://doi.org/10.1016/ .jhydrol.2005.07.032. 2006.

964 Dehaan, R., and Taylor, G.: Field-derived spectra of salinized soils and vegetation as
965 indicators of irrigation-induced soil salinization, Remote Sens Environ, 80(3),
966 406-417. https:// doi.org/10.1016/S0034-4257(01)00321-2. 2002.

967 Delonge, K. C., Ascough, J. C., Andales, A. A., Hansen, N. C., Garcia, L. A., Arabi, M.:
968 Improving evapotranspiration simulations in the CERES-Maize model under
969 limited irrigation. Agr Water Manage, 115: 92-103. http://doi.org/
970 10.1016/j.agwat.2012.08.013. 2012.

971 Doherty, J. and Simmons C.: Groundwater modelling in decision support: reflections
972 on a unified conceptual framework, Hydrogeol. J, 21(7), 1531-1537. https://
973 doi.org/10.1007/s10040-013-1027-7. 2013.

974 Feng, Z., Wang, X., Feng, Z.: Soil N and salinity leaching after the autumn irrigation
975 and its impact on groundwater in Hetao Irrigation District, China. Agr Water
976 Manage, 71(2): 131-143. https:// doi.org/10.1016/j.agwat.2004.07.001. 2005.

977 Flint, A.L., Flint, L.E., Kwicklis, E.M., Fabryka-Martin, J.T., and Bodvarsson, G.S.:
978 Estimating recharge at Yucca Mountain, Nevada, USA: comparison of methods.
979 Hydrogeol. J., 10:180-204. https:// doi.org/ 10.1007/s10040-001-0169-1. 2002.

980 Gao, X., Huo, Z., Bai, Y., Feng, S., Huang, G., Shi, H., and Qu, Z.: Soil salt and
981 groundwater change in flood irrigation field and uncultivated land: a case study
982 based on 4-year field observations. Environ. Earth Sci., 73:2127-2139. https://
983 doi.org/10.1007/s12665-014-3563-4. 2015.

984 Gao, X., Huo, Z., Qu, Z., Xu, X., Huang, G., and Steenhuis, T.S.: Modeling
985 contribution of shallow groundwater to evapotranspiration and yield of maize in
986 an arid area. Sci. Rep-UK 7. https:// doi.org/10.1038/srep43122. 2017.

987 Gardner, W.: Some study-state solutions of the unsaturated moisture flow equation
988 with application to evaporation from a water table. Soil Sci., 85:228-232. 1958.

989 Gardner, W., Hillel, D., and Benyamini, Y.: Post-Irrigation Movement Soil Water 1.
990 Redistribution. Water Resour Res., 6:851-860. https:// doi.org/
991 10.1029/WR006i003p00851. 1970a.

992 Gardner, W., Hillel, D., and Benyamini, Y.: Post-Irrigation Movement of Soil Water 2.
993 Simultaneous Redistribution and Evaporation. Water Resour Res., 6:1148-1153.
994 https:// doi.org/ 10.1029/WR006i004p01148. 1970b.

995 Guo, S., Ruan, B., Chen, H., Guan, X., Wang, S., Xu, N. and Li, Y.: Characterizing the
996 spatiotemporal evolution of soil salinization in Hetao Irrigation District (China)
997 using a remote sensing approach. Int J Remote Sens 39: 6805-6825. https://
998 doi.org/10.1080/01431161.2018.1466076. 2018.

999 Hanson, B., Hopmans, J., Šimůnek, J.: Leaching with Subsurface Drip Irrigation
1000 under Saline, Shallow Groundwater Conditions. Vadose Zone J. 7, 810-818.
1001 http://doi.org/10.2136/vzj2007.00532008. 2008.

1002 Hsiao, T., Heng, L., Steduto, P., Rojas-Lara, B., Raes, D., Fereres, E.: AquaCrop-The
1003 FAO Crop Model to Simulate Yield Response to Water: III. Parameterization and
1004 Testing for Maize. Agron. J, 101(3):448-459. https:// doi.org/
1005 10.2134/agronj2008.0218s. 2009.

1006 Hu, S., Shi, L., Huang, K., Zha, Y., Hu, X., Ye, H., Yang, Q.: Improvement of
1007 sugarcane crop simulation by SWAP-WOFOST model via data assimilation.
1008 Field Crop Res., 232: 49-61. https:// doi.org/10.1016/j.fcr.2018.12.009. 2019.

1009 Huang, Q., Xu, X., Lu, L., Ren, D., Ke, J., Xiong,Y., Huo, Z. and Huang, G.: Soil
1010 salinity distribution based on remote sensing and its effect on crop growth in

Hetao Irrigation District. Transactions of the Chinese Society of Agricultural Engineering, 34:102-109. 2018.

Kendy, E., Gérard-Marchant, P., Walter, M. T., Zhang, Y., Liu, C., and Steenhuis, T.S.: A soil-water-balance approach to quantify groundwater recharge from irrigated cropland in the North China Plain. Hydrol. Process., 17:2011-2031. https:// doi.org/10.1002/hyp.1240. 2003.

Leube, P. C., : Temporal moments revisited: Why there is no better way for physically based model reduction in time, Water Resour Res, 48(11): W11527. https:// doi.org/10.1029/2012WR011973 2012.

Li, J., Pu, L., Han, M., Zhu, M., Zhang, R., Xiang, Y.: Soil salinization research in China: Advances and prospects, J Geogr Sci, 24(5), 943-960. https:// doi.org/ 10.1007/s11442-014-1130-2 .2014

Letey, J., Hoffman, G.J., Hopmans, J.W., Grattan, S.R., Suarez, D., Corwin, D.L., Oster, J.D., Wu, L., Amrhein, C.: Evaluation of soil salinity leaching requirement guidelines. Agric. Water Manag. 98, 502–506. https://doi.org/10.1016/j.agwat.2010.08.009. 2011.

Li, X., Zhao, Y., Xiao, W., Yang, M., Shen, Y., Min, L.: Soil moisture dynamics and implications for irrigation of farmland with a deep groundwater table. Agr. Water Manage.,192:138-148. https:// doi.org/ 10.1016/j.agwat.2017.07.003.2017.

Liu, J.: A GIS-based tool for modelling large-scale crop-water relations. Environ Modell Softw. 24(3): 411-422. https:// doi.org/ 10.1016/j.envsoft.2008.08.004. 2009.

Liu, Z., Wang, X., Huo, Z, Steenhuis, T.S.: A unique vadose zone model for shallow aquifers: the Hetao irrigation district, China. Hydrol Earth Syst Sc. 23(7):3097-3115. https:// doi.org/ 10.5194/hess-23-3097-2019. 2019.

Luo, Y., and Sophocleous, M.: Seasonal groundwater contribution to crop-water use assessed with lysimeter observations and model simulations. J. Hydrol, 389:325-335. https:// doi.org/10.1016/j.jhydrol.2010.06.011. 2010.

Ma, Y., Feng, S., and Song, X.: A root zone model for estimating soil water balance and crop yield responsesto deficit irrigation in the North China Plain. Agr. Water Manage., 127:13-24. https:// doi.org/10.1016/j.agwat.2013.05.011. 2013.

Miao, Q., Rosa, R., Shi, H., Paredes, P., Zhu, L., Dai, J., Goncalves, J., Pereira, L.: Modeling water use, transpiration and soil evaporation of spring wheat–maize and spring wheat–sunflower relay intercropping using the dual crop coefficient approach. Agr Water Manage, 165:211-229. https://doi.org/10.1016/j.agwat.2015.10.024.2016.

Minhas, P., Ramos, T., Ben-Gal., A., Pereira, L.: Coping with salinity in irrigated agriculture: Crop evapotranspiration and water management issues. Agr Water Manage, 227, 105832. https://doi.org/ 10.1016/j.agwat.2019.105832. 2020.

Moriasi, D. N., Arnold, J. G., Van Liew, M. W., Bingner, R. L., Harmel, R. D., Veith, T. L.: Model evaluation guidelines for systematic quantification of accuracy in watershed simulations. T ASABE, 50(3): 885-900. 2007.

Nash, J.E., and Sutcliffe, J.V.: River flow forecasting through conceptual models part I – a discussion of principles. J Hydrol. 10:282-290. 1970.

Novark, V.: Estimation of Soil-water Extraction Patterns by Roots, Agr Water Manage, 12(4), 271-278. https:// doi.org/10.1016/0378-3774(87)90002-3. 1987

Phogat, V., Mallants, D., Cox, J., Šimůnek, J., Oliver, D., Awad, J.: Management of soil salinity associated with irrigation of protected crops. Agr. Water Mange., 227:105845. https://doi.org/10.1016/j.agwat.2019.105845.2020.

Raes, D., Steduto, P., Hsiao, T., Fereres.: AquaCrop-The FAO Crop Model to Simulate Yield Response to Water: II. Main Algorithms and Software Description, Agron. J, 101(3), 438. https:// doi.org/10.2134/agronj2008.0140s.2009.

Regis, R., and Shoemaker, C.: Constrained Global Optimization of Expensive Black Box Functions Using Radial Basis Functions, J Global Optim, 31(1), 153-171. https:// doi.org/10.1007/s10898-004-0570-0. 2005.

Ren, D., Xu, X., Hao, Y., and Huang, G.: Modeling and assessing field irrigation water use in a canal system of Hetao, upper Yellow River basin: Application to maize, sunflower and watermelon. J. Hydrol, 532:122-139. https:// doi.org/10.1016/j.jhydrol.2015.11.040. 2016.

Ren, D., Xu, X., Romos, T., Huang, Q., Huo, Z., Huang, G.: Modeling and assessing the function and sustainability of natural patches in salt-affected agro-ecosystems: Application to tamarisk (Tamarix chinensis Lour.) in Hetao, upper Yellow River basin. J. Hydrology.

532:490-504.https://doi.org/10.1016/j.jhydrol.2017.04.054.2017.

Rengasamy, P.: World salinization with emphasis on Australia, J Exp. Bot., 57(5), 1017-1023. https:// doi.org/10.1093/jxb/erj108 .2006

Rhoades, J., Manteghi, N., Shouse, P., Alves, W.: Soil Electrical Conductivity and Soil Salinity: New Formulations and Calibrations, Soil Sci. Soc. Am. J., 53(2): 433-439. https:// doi.org/ 10.2136/sssaj1989.03615995005300020020x. 1989.

Ritter, A., and Muñoz-Carpena, R.: Performance evaluation of hydrological models: Statistical significance for reducing subjectivity in goodness-of-fit assessments. J Hydrol., 480:33-45. 2013.htt p:// doi.org/ 10.1016/j.jhydrol.2012.12. 004. 2013.

Rosa, R.D., Paredes, P., Rodrigues, G.C., Alves, I, Fernando, R.M., Pereira, L.S., Allen, R.G.: Implementing the dual crop coefficient approach in interactive software. 1. Background and computational strategy. Agr. Water Manage., 103: 8-24. https:// doi.org/10.1016/j.agwat.2011.10.013. 2012.

Sau, F., Boote, K., Bostick, W., Jones, J., Minguez, M.,: Testing and improving evapotranspiration and soil water balance of the DSSAT crop models. Agron. J., 96: 1243-1257. https:// doi.org/ 10.2134/agronj2004.1243. 2004.

Shelia, V., Simunek, J., Boote, K., Hoogenbooom, G.: Coupling DSSAT and HYDRUS-1D for simulations of soil water dynamics in the soil-plant-atmosphere system. J Hydrol Hydromech., 66(2): 232-245. https:// doi.org/10.1515/johh-2017-0055. 2018.

Šimůnek, J., Šejna, M. and van Genuchten, M.T.: The HYDRUS-1D software package for simulating the one-dimensional movement of water, heat, and multiple solutes in variably-saturated media. Version 2.0. IGWMC-TPS-70. Int. Groundwater Modeling Ctr., Colorado Schoolof Mines, Golden. 1998.

Steduto, P., Hsiao, T., Raes, D., Fereres, E.: AquaCrop-The FAO Crop Model to Simulate Yield Response to Water: I. Concepts and Underlying Principles. Agron J., 101(3):426-437. https:// doi.org/10.2134/agronj2008.0139s. 2009.

Steenhuis, T., Richard, T., Parlange, M., Aburime, S., Geohring, L., PArlange, J.: Preferential Flow Influences on Drainage of Shallow Sloping Soils. Agr Water Manage., 14(1-4):137-151. https:// doi.org/ 10.1016/0378-3774(88)90069-8. 1988.

Uehara, G.: Technology-transfer in the tropics. Outlook Agr., 18(1): 38-42. https:// doi.org/ 10.1177/003072708901800107. 1989.

Van Diepen, C., Wolf, J., van Keulen, H., Rappoldt, C.: WOFOST A STIMULATION MODEL OF CROP PRODUCTION. Soil Use and Management, 5(1): 16-24. 1989.

Wallender, W. , Tanji, K. : Agricultural salinity assessment and management. Agricultural salinity assessment and management. Ed.2. American Society of Civil Engineers (ASCE), Reston, USA. University of California-Davis, USA.: xxx+1094pp. 2011.

Wang, X., Huang, G., Yang, J., Huang, Q., Liu, H., Yu, L.: An assessment of irrigation practices: Sprinkler irrigation of winter wheat in the North China Plain. Agr Water Manage., 159: 197-208. https:// doi.org/ 10.1016/j.agwat.2015.06.011. 2015.

Wang, J., Huang, G., Zhan, H., Mohanty, B., Zheng, J., Huang, Q., Xu, X.: Evaluation of soil water dynamics and crop yield under furrow irrigation witha two-dimensional flow and crop growth coupled model. Agr Water Manage., 141: 10-22. https:// doi.org /10.1016/j.agwat.2014.04.007. 2014.

Wu, X., Zheng, Y., Wu, B., Tian, Y., Han, F., Zheng, C.: Optimizing conjunctive use of surface water and groundwater for irrigation to address human-nature water conflicts: A surrogate modeling approach. Agr Water Manage, 163(1): 380-392. https:// doi.org/10.1016/j.agwat.2015.08.022. 2016.

Williams, J., Jones, C., Kiniry, J., and Spanel, D.: The EPIC Crop Growth Model. T. ASAE, 32:479-511. 1989.

Willcox, K., and Peraire J.: Balanced Model Reduction via the Proper Orthogonal Decomposition, AIAA J, 40(11), 2323-2330. https:// doi.org/10.2514/2.1570. 2002.

Xu, X., Sun, C., Qu, Z., Huang, Q., Ramos, T.B., and Huang, G.: Groundwater Recharge and Capillary Rise in Irrigated Areas of the Upper Yellow River Basin Assessed by an Agro-Hydrological Model. Irrig. Drain., 64:587-599. https:// doi.org/10.1002/ird.1928. 2015.

Xu, X., Sun, C., Huang, G., Mohanty, B.: Global sensitivity analysis and calibration of parameters for a physically-based agro-hydrological model. Environ Modell Softw., 83: 88-102. https:// doi.org/10.1016/j.envsoft.2016.05.013. 2016.

1137 Xu, X., Huang, G., Sun, C., Pereira, L., Ramos, T., Huang, Q., Hao, Y.: Assessing the
1138 effects of water table depth on water use, soil salinity and wheat yield: Searching
1139 for a target depth for irrigated areas in the upper Yellow River basin. Agr Water
1140 Manage, 125: 46-60. https:// doi.org/10.1016 /j.agwat.2013.04.004. 2013.

1141 Xu, X., Huang, G., Qu, Z., and Pereira, L.S.: Assessing the groundwater dynamics
1142 and impacts of water saving in the Hetao Irrigation District, Yellow River basin.
1143 Agr Water Manage., 98:301-313. https:// doi.org/10.1016/j.agwat.2010.08.025.
1144 2010.

1145 Xue, J., Huo, Z., Wang, F., Kang, S., and Huang, G.: Untangling the effects of shallow
1146 groundwater and deficit irrigation on irrigation water productivity in arid region:
1147 New conceptual model. Sci. Total Environ., 619-620:1170-1182. https://
1148 doi.org/10.1016/j.scitotenv.2017.11.145 2018.

1149 Yang, X., Chen, Y., Pacenka, S., Gao, W., Ma, L., Wang, G., Yan, P., Sui, P., and
1150 Steenhuis, T. S.: Effect of diversified crop rotations on groundwater levels and
1151 crop water productivity in the North China Plain, J. Hydrol., 522, 428–438,
1152 https://doi.org/10.1016/j.jhydrol.2015.01.010, 2015a.

1153 Yang, X., Chen, Y., Pacenka, S., Gao, W., Zhang, M., Sui, P., and Steenhuis, T. S.:
1154 Recharge and groundwater use in the North China Plain for six irrigated crops for
1155 an eleven year period, Plos One, 10, e0115269, http://doi.org/10.1371/journal.
1156 http:// doi.org/10.1371/10.1371/journal.pone.0115269, 2015b.

1157 Yeh, P.J., and Famiglietti, J.S.: Regional groundwater evapotranspiration in Illinois. J.
1158 Hydrometeorol., 10:464-478. https:// doi.org/ 10.1175/2008JHM1018.1. 2009.

1159 Zhang, B., Kang, S., Zhang, L., Du, T., Li, S., Yang, X.: Estimation of seasonal crop
1160 water consumption in a vineyard using Bowen ratio-energy balance method.
1161 Hydrol. Process, 21(6): 3635-3641. https:// doi.org/ 10.1002/hyp.6568.

1162 Zhang, F., Zhou, G., Wang, Y., Yang, F., Nilsson, C.: Evapotranspiration and crop
1163 coefficient for a temperate desert steppe ecosystem using eddy covariance in
1164 Inner Mongolia, China. Hydrol. Process, 26(3): 379-386. https:// doi.org/
1165 10.1002/hyp.8136.